ABDULAI MUSAH (ID No: 40192)

MODELING AND SIMULATION OF STRESS DISTRIBUTION AND CRACK CONFIGURATION OF THE GEOMETRY OF CERAMIC WATER FILTER

A THESIS

SUBMITTED TO THE GRADUATE FACULTY

IN PARTIAL FULFILLMENT OF THE REQUIREMENT FOR THE

DEGREE OF

MASTER OF SCIENCE

DEPARTMENT OF MATERIALS SCIENCE AND ENGINEERING

SUPERVISOR: PROF. WINSTON WOLE SOBOYEJO

DECEMBER, 2011.

ACKNOWLEGEMENTS

I will first of all thank the Almighty Allah for seeing me through to this work.

I would like to express my thanks to my project advisor, Prof.W.Soboyejo for his guidance and support throughout the duration of this research, without his encouragement and expertise this project would not have been possible. I would also like to extend my gratitude to my Parents for their care and support throughout my education. Also to all my lecturers whose effort and dedication brought me to this far I say thank you. Finally to all my friends who in one way or the other supported me in this work.

Table of Contents

List of Tables Pages

List of figures

Abstract

Most countries in Africa are faced with difficult challenges in terms of providing safe, clean drinking water for their citizens. The world Health organization estimates that approximately 500 lives are lost per day in Nigeria from water related diseases while globally, 1.1 billion lack access to improve water supplies. Point-Of-use water treatment technologies, such as household ceramic water filters, offer an affordable and effective means of treating water to standards suitable for drinking. The fact that ceramic water filter can be produced locally with local material makes it attractive as a point-of-use treatment technology that is affordable, appropriate and sustainable.

Ceramics are brittle and therefore Ceramic water filters are faced with the issue of breakages and rupture during transportation and usage. The focus of this study is on using finite element method with the aid of Abaqus software to model and simulate the stress distribution and crack behavior within the geometry of ceramic water filter. Also try to come out with the optimum choice of filter geometry that can be used by producers of ceramic water filter to help address the rampant breakages and rupturing of water filters. Three shapes of geometry were considered in this study. These are the frustum shape, the cylindrical (circle) and the rectangular (square) base shape. Recommendations for future work include the maximum impulse force before fracturing and the critical thickness for reservoir.

CHAPTER ONE

1.0 INTRODUCTION

1.1 BACKGROUND

The world community still faces a hard challenge: to have more than halved the number of people without access to improve water supply and sanitation by the year 2015. This is also one of the millennium Development Goals that was committed to by governments from worldwide during the world 2002 summit on Sustainable Development in Johannesburg South Africa (1). The quantity and quality of water is necessary for life. One sixth of the world's population as at 2000, estimated to be 1.1 billion people, lack access to good drinking water supply and two fifths, or 2.4 billion people, lack access to good sanitation (2).Roughly, 3.4 million people are reported to die annually from water related diseases, these are mostly children under the age of five (3).Diarrhea diseases alone account for 2.1 million deaths.

The millennium Development Goal for water is still working out ways of getting and delivering access to good treated water supply by the year 2015(4).The achievements of this ambitious goal by the world nations by the year 2015 through the conventional centralized system approached is quiet doubtful. This is because the conventional system is quiet expensive and cannot be afford by all.

In attempts of finding ways to providing treated drinking water that can be affordable to all, the point- of –use household water treatment systems were initiated to complement the

conventional centralized water supply systems. One of such initiative is the Ceramic water filter. It offers affordable and effective ways of treating water to a standard and suitable for drinking. Though its usage goes back to centuries, little has been done about the documentation, testing of the effectiveness of low-cost ceramic water filters both in the laboratory and in the field, physical and mechanical properties of ceramic water filter and the best choice of geometry to be used in order to solved the issue of breakages during distribution and service, and health impact of using these ceramic water filters (5).

The use of clay ceramic water filters for water treatment has impacted the occurrence of water borne diseases across Africa, Asia, and South America (6,7). Clay and plant by-products, such as sawdust, agricultural residues, husk from rice and coffee etc mixed in some composition are used as base materials to produce these filters .The mixture is moistened, molded dried and eventually fired to produce porous clay ceramic materials as well as filtration devices.(8)

Altering the composition change the microstructural and mechanical properties of the filters. The flow of microstructural and the mechanical features also change geo-spatially because of lack of similar raw material constituents at different places globally (8,-9). The porosity, density and the stress distribution play a great role in determining the strength of ceramic water filters. This has led to functional challenges such as water contamination, loading rate, application frequency, flow rate, material availability and composition are not the same worldwide. These therefore, contribute to variability in the physical and mechanical properties of clay ceramic water filters. Clay ceramic are known to be brittle, so adding organic or inorganic materials can controlled and optimize the structural integrity of ceramic water filters produce from them.

Also influencing the firing temperature can also controlled the strength of the water filter. As mention earlier, during transportation ceramic water filters got broken and ruptures also occurred during used.(7,10,11, 12)

Finite Element Analysis (FEA) is a numerical method which provides solution to problem that would be difficult to obtain. It is the most widely applied computer simulation method in engineering. In fracture mechanics, it is most often used in determination of stress intensity factors, however the applications of this method is in much broader range of areas such as Arospace,Civil and Automobile Engineering to do Structure analysis, thermal or fluid flows analysis etc. It also plays a very vital role in Electromagnetics, Geomechanics and Biomechanics.(13).The FEA allows more complex element analysis to be modeled. The finite element method (FEM) was originally an extension of matrix analysis, developed by structural engineers. It has since been used in every field where differential equations define the problem behavior (14).

1.2 Problem Statement

Though a lot of research has been carried out on ceramic water filters: for bacteria, fluoride, pathogenic removal and the physical properties of porous ceramic filter, there are currently, no work done on the best choice of geometry and the stress distribution and crack configuration within the geometry of the ceramic water filter.

1.3 Scope of work

This research is focus on providing better understanding of the stress distribution within the geometry and identifying the region of maximum stress and maximum stress value using finite element model and explore the best alternative of geometry. It would also look at possible crack configuration and determine the fracture toughness and J-integral and determine condition at which failure occurs. The stress distribution values would be used to calculate fracture toughness, for Neumann Raju semi elliptical and corner crack and identify the best filter design for crack growth resistance.

Chapter Two

Literature Review

2.1 Point-Of- Used Household Ceramic Water treatment Technologies.

Most people – predominately women- spend most of their times during the day collecting, carrying and storing water for drinking. These waters are mostly not from any water treatment plant and supply system but from various sources including local dug wells, springs and stone taps. These waters if not contaminated from the source, may become contaminated along the line of transportation or during storage before consumption .In developing countries like Nigeria; ensuring safe drinking water is the duty of individual members of the community. This has made the household water treatment technology as ways to get meaningful clean drinking water. Recent studies indicated that household water treatment seems to be gaining ground especially within the International Development organizations like the World Health organization (WHO) and the UNICEF [2].

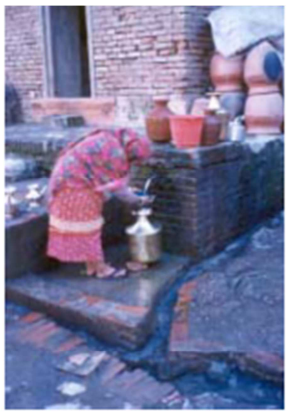

Nepali Woman Collecting Drinking Water from a Stone Tap

Thimi, Nepal. January 2003.

Ceramic water filter is one of such household treatment technology which is less-costly and very effective at improving the quality of water. A variety of technologies are being used in the manufacturing of ceramic water filters. They are mostly doped with non-poisonous chemicals to enhance the health impact of the filter.

2.1.1 Ceramic water filter doped with Colloidal Silver.

The basic materials used in the manufacturing of ceramic water filters are clay, water, combustible material, and grog. These materials undergo process like grinding and sieving before they are mixed together into a uniform mixture, pressed or molded into a filter shape. It is dry and deep into Colloidal Silver as bactericide. It is the last step after the filter has been fired and dried.[3]

A summary of the materials used in the manufacturing of CWF is shown in the below.

Material	Brief Description	Examples
Clay	➢ Clays are fine-particulate geologic materials that have the unique property of being plastic when wet and hard when fired. Their plasticity allows ceramist to form shapes that maintain their form before being fired. Once fired, the clay hardens and the shape becomes permanent.	- White kaolin clay from India - Red clay from Thimi, Nepal - Black clay from Bhaktapur, Nepal
Water	➢ Controls workability/ plasticity as well as shrinkage	
Combustible Material	➢ Used to increase the porosity of the ceramic since the combustible material will burn off during the firing, leaving behind pores or voids through which water will travel.	- Sawdust (e.g.: oak, pine) - Flour (e.g.: wheat flour, corn flour) - Rice husk ash
Temper or Grog	➢ Temper is defined as all non-plastic material used to reduce shrinkage/warpage and to control porosity to some extent. The term grog is used more frequently in the production of ceramic water filters and refers to pre-fired ceramic material that is mixed with raw clay, water, and/or combustible material to form a ceramic filter unit.	- Ground bricks - Pre-fired disk that is ground and sieved (see Grog Section 4.1.3.
Colloidal Silver	➢ Colloidal silver consists of silver particles suspended in distilled water or proteins. It is coated onto the surface of the filter element after it has been fired and dried. CS is used as a disinfectant to help reduce microbial contamination.	- Microdyn (Mexican product)

Fig.1 Robert Dies,2001

The basic equipment needed for the production of CWFs is the grinder, Screens, Mixers, Filter Press and Molds. Others include Kiln, Buckets and Scales and Surface or Storage Area.

2.1.1.1 Manufacturing Process

The materials usually clay and sawdust are grinded to a more uniform and smaller grain. They are mixed and form moistened suspension of clay and sawdust in a given composition by volume. The plasticity present in the moistened of the mixture allows it to be molded under stress to any shape as needed [3].The filters are cast usually into frustum shape of given dimensions. They are sintered around 900^{o}C to introduce pores into the mold serving its filtration purposes[3].Colloidal Silver is used to paint onto the surface of the filters after firing and drying has been done[1 and 4]. This would disinfect it and help to remove bacterial and microbial infection [5].

Summary of ceramic Water filter Production base on Madhyapur clay crafts in Thimi, Nepal.

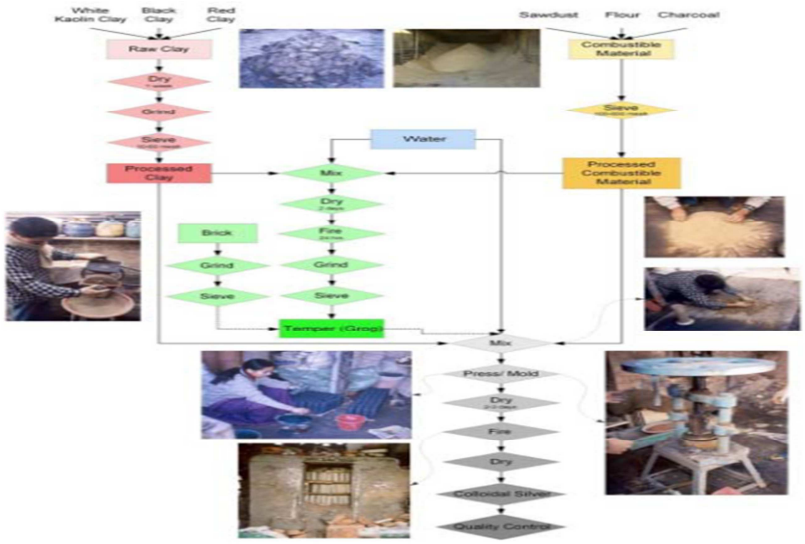

Fig.1

In a work by Robert Dies, 2003, at the Massachusetts Institute of technology, three types of filters were produced and tested in order to see which geometry is efficient in bacteria removal. The summary of the test perform is shown in the figure.

Test Number	Filters Tested	# of Filters Tested	Raw Water Concentration (cfu/100 mL)	
			Total Coliform	*E.coli*
1. Candles	Katadyn® candle filters (Ceradyn and Gravidyn); Hari candle filters (1 coated with CS; 1 without); and Hong Phuc candle filter.	5	89	56
2. Hari Disks	Hari white clay disk filters (4: 2 coated with CS; 2 without)	4	2,861	1,550
3. Reid Disks	Reid Harvey Grog Disk Filters (4 red clay + red clay grog: 2 coated with CS; 2 without. 4 black clay + red clay grog: 2 coated with CS; 2 without)	8	2,500	1,561

Table 2

The period of six hours were used by each of the three test carried out. The filters were soaked overnight with tap water to make them saturated before the test.The bucket were then clean with soap and water and allowed to dry for one to two hours. The filter element was cleaned by light brushing the surface of the filter with an abrasive scrub brush.

The filters were filling with raw water to a height of 240mm for candle and 170mm for disk filters. They were left for two to three hours to allow water to be collected in the lower

container. Sample for microbial analysis was taken from this water. The water collected within the interval of three hours. This mostly is influence by the time the lower containers are filled. Sample collected were analyzed within one hour in the laboratory.

The flow rate calculation was done using the relation

$$\text{Flow rate} = \frac{volume\ of\ water\ measure\ at\ time\ T(mL)}{Elapsed\ time, T\ from\ start\ of\ test\ (hours)} \qquad (1)$$

The average flow rate for Hari Clay disk without colloidal silver is 377mL/hr and with colloidal silver is 353mL/hr and that of Reid red Clay disk is 850mL/hr and 756mL/hr respectively. The black clay disk shows 412mL/hr and 341mL/hr respectively.

The microbial removal efficiency was carried out in terms of Log reduction value as indicated below

$$\text{Log Reduction Value (LRV)} = \frac{\log_{10}(untreated)}{\log_{10}(treated)} \qquad (2)$$

$$\text{\% Removal efficiency} = \frac{untreated - treated}{untreated}\ 100 \qquad (3)$$

Untreated is the sample from the raw water and the treated is from the filtered water.

Transport Simulations. Effluent tracer and bacteria concentrations over time for ceramic filter with and without colloidal- silver treatments were simulated using the following transient one-dimensional form of the advection-dispersion equation with first-decay:

$$\mathbb{R}\frac{\partial c}{\partial t} = D\frac{\partial^2 c}{\partial x^2} - v\frac{\partial c}{\partial x} - \mu c \qquad (4)$$

Subject to the following initial boundary conditions

C ($x, 0) = 0$

C (0, t) = C_o for t < t_o

C (0, t) = 0 for t > t_o $\qquad \frac{\partial C(L,t)}{\partial x} = 0$

Where R is the retardation coefficient, c is the concentration of [3H]H_2O (counts per minute per mL) or E.coli (mpn/100mL),t is the time, to is the tracer or bacteria pulse injection time, D is the dispersion coefficient(cm^2min-1),x is the distance(cm),v is the linear velocity(cm/min),μ is the first-order decay coefficient(1/min), and L is the thickness of the filter. The model assumes local equilibrium sorption. The computer program CXTFIT(18) was applied to provide appropriate fit of the model to the experimental data and v for each column were found from the 3[H]H_2O transport experiment(where R=1and μ=0).R and μ were found from the E.coli experiments. μ =0 for untreated filter with colloidal silver [6]

TABLE 1. Physical Properties and Bacteria-Transport Model Parameters for Ceramic Filters Fabricated Using Guatemalan, Redart, and Mexican Soils

	Guatemala	Redart	Mexico
hydraulic conductivity (cm/s)	1.15×10^{-5}	5.01×10^{-5}	3.26×10^{-5}
porosity (%)	38.8	41.9	37.4
median pore diameter (μm)	8.21	2.03	14.3
	tracer transport		
linear velocity, v (cm/min)	0.058	0.050	0.068
coefficient of hydrodynamic dispersion, D (cm^2/min)	0.021	0.005	0.013
	bacteria transport through filters without colloidal silver		
rejection mass, R_{mass} (dimensionless)	0.9867	0.9997	0.9786
retardation factor, R	1.04	0.68	0.79
	bacteria transport through filters with colloidal silver		
first-order decay coefficient for painted filters, μ (min^{-1})	0.008	0.0008	0.008
first-order decay coefficient for submerged filters, μ (min^{-1})	0.015	N.C.*	0.017

* N.C. - Not Calculated (since no bacteria were detected in effluent).

Table.3.(oyandel-craver-and-smith,2008)

2.1.2 Ceramic filter Doped with Iron Oxide

In 2010, Nadia H. et al, introduced a filter known as Fe- CWFs. This is to reduce if not eliminate the consumption of arsenic element through water. This filter has Fe_2O_3 added to it during production. The Fe_2O_3 is noted to have the highest viral adsorption ability among the ceramic impregnated with various metal oxide [7].The Fe_2O_3 removed 4.6 to 5.6log of MS2 bacteriophage with 3.5 log irreversible. However the FeOOH adsorb more than 8.0 log both MS2 and X-174 bacteriophage irreversibly.

Three types iron: clay filter was manufacture and fired to about 861^{o}C. These filters are 1:8,2:7 and 3:6 representing 11 volume %,22 volume% and 33 volume% iron oxide respectively. To determine the species of oxide present, the powdered XRD of the iron oxide used were taken before and after firing to the temperatures of 700^{o}C,800^{o}C and 900^{o}C.This is to see if there exists a phase change during firing. The results showed a unique pattern of quartz (SiO_2) in both the fired and the unfired iron oxide. Also FeOOH was present in the unfired whiles the fired

show peaks for α-Fe_2O_3irrespective of the firing temperature. Interestingly, this was found to match with the literature;dehydroxylation of FeOOH to Fe_2O_3that begins at 240^{o}C[8].When the EDX of both the iron oxide and the Red Art clay was taken ,they showed the elemental composition of the clay as;54.3wt%SiO_2,24.5wt%Al_2O_3,11.6wt%Fe_2O_3,5.3wt%K_2O with some minor ones. Iron oxide, when fired also displayed 72.1wt% Fe_2O_3, 15.5 wt%SiO_2, and 7.5wt% Al_2O_3.Presented in Table 3 is the name of filter base on volume and the quantity of Fe_2O_3 in wt%.

Filter Name (vol % Fe Added)	Total Iron Oxide (wt %)
0	11.6
11	18.2
22	24.9
33	31.6

Table.4

(Nadia H. et al,2010). Table Total iron oxide weight percentages for test filters.

With regard to bacteriophage removal efficiency, the results indicated that the addition of Fe_2O_3 led to a high viral removal efficiency of the filters. The best filter (Fe:CWF,22% Vol) was able to remove 1.93 log of viral challenge as compared to the control which removed 0.87 log of MS2.They were both started with viral load of ~10^7puf/mL.

Fe-CWF	Log Removal (log)	95% CI (log)	% Removal (%)	95% CI (%)	p Value	n
0%	0.87	0.55–1.19	86.53	72.04–93.51	------	7
11%	1.50	1.34–1.65	96.81	95.48–97.75	5.93×10^{-3}	7
22%	1.93	1.76–2.10	98.83	98.26–99.21	2.20×10^{-4}	7
33%	1.28	1.07–1.40	94.18	91.43–96.05	3.23×10^{-2}	5

Table.5 (Nadia et al, 2010)

Table showing log reduction of the various filters.

Filter	Log Removal (log)	95% CI (log)	% Removal (%)	95% CI (%)	p Value	n
0%	3.26	2.85–3.67	99.95	99.86–99.98	------	3
11%	4.10	3.12–5.09	99.99	99.92–99.999	0.231	3
22%	3.57	3.14–4.00	99.97	99.93–99.99	0.369	3
33%	3.22	3.03–3.40	99.94	99.91–99.96	0.847	3

Table6 (Nadia et al, 2010)

Table for E.coli filtration of Fe-CWF experiment.

Figure showing the log reductions of iron oxide in wt%.

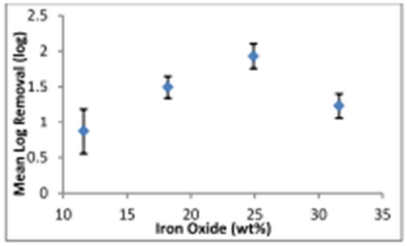

Fig2. (Nadia H. et al,2010.)

Some were of the opinion that the addition of Fe_2O_3 may increase the sizes of the filters. But the result on bacteria removal efficiency was still high of about 3 log(99.9%), as indicated in the figure.

Fig 3. 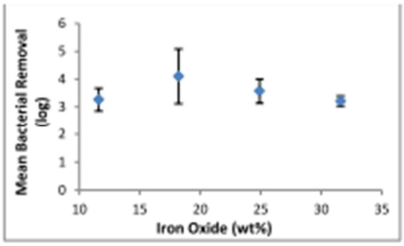

(Nadia.H.et al,2010)

Comparison of the bacterial removal efficiencies of the Fe-CWFs with regard to Fe_2O_3concentration.

This means that despite the increased in the sizes of the porous ceramic upon the addition of Fe_2O_3,

It was able to remove almost 99% of viral contamination whiles maintaining 99.94 to 99.99% bacterial removal efficiencies.

2.1.3 Ceramic Filter Doped with Hydroxyapatite

In another development, Yakub et al, 2010,in attempt to remove the overdose consumption of fluoride by the body through water, introduced the used of Hydroxyapatite chemical to be used in clay during the Ceramic Water filter manufacturing.

Fluoride is present in all natural water. The intake of fluoride into the body in rightful amount has many beneficial effect which includes enhancing healthy teeth and preventing dental cavaties.On the contrary, it may lead to serious effects when its concentration is high and consumed over long period. One of such effect is dental fluorosis that is feature by staining, pitting and mottling of the enamel. In some cases, it can lead to crippling skeletal fluorosis and osteoporosis (Inyang,2004:Mandinic et aal.,2010).

The mechanism involved in removing fluoride from water is through the process of adsorption, precipitation and ion exchange. Though work has been done on Hydroxyapatite(HA) by Parker, Fan and Smith,2003,C.Sairam Sundaram,2008 and Alagumuthu, Veeraputhiran, & Venkataraman, 2010.it was non-sintered. In Yakub et al, it sintered the mixture of clay and HA heterogeneously.

Five types of different adsorbent were produced and have changing proportion of clay to HA.These are 0:100,75:25,80:20,90:10 and 100:0.Sawdust is added in the ratio of C:HA as 2;1, ie C+HA:S. The adsorbents sintering temperature were 500^{o}C, 600^{o}C, 700^{o}C, 800^{o}C and 900^{o}C.

In studying the effectiveness of substances, three types filter with frustum shape were manufactured. The composition of clay to HA be 75:25, 80:20 and 100:0 and sawdust added in the ratio of 2:1 by volume.

In looking at the effect of sintering temperature on HA, the quantity of fluoride adsorbed at equilibrium were used. This is given as;

$$Qe = mg/g \qquad (5)$$

Mg= mass of fluoride adsorbed and g= mass of adsorbent.

It is also define as;

$$Qe = 10^{-3}(C_i - C_e)\, Vxm \qquad (6)$$

C_i = initial concentration of fluoride

C_e= concentration of fluoride at equilibrium

V= volume of fluoride solution

M= mass of adsorbent used.

It was shown graphically in this work that adsorption ability of “HA only “decreases in step-wise manner as the sintering temperature goes high.

Sawdust was burn off during sintering at 450^{o}C to 550^{o}C. The HA produce was white but get darker after sintering with sawdust. The HA sintered became continuously lighter while sintering and was almost white completely at 900^{o}C.This showed that as the sintering temperature increases the carbon residue in sawdust get reduce. That is to say at low temperature the residual carbon in the form of activated carbon is partially responsible for the adsorption ability of HA. This was why as the sintering temperature goes high the adsorption ability of HA decreases.

In looking at the effect of HA content, it reported that the higher the content of HA, the greater the quantity of fluoride adsorbed. HA has the ability of removing fluoride ion in water and does that by the formation of fluroapatite, ion exchange and formation of calcium fluoride. Also the clay, which is made up illite and kaolinite, does the ion exchange when treated with fluoride ion and by the method of hydration of metal oxides in aqueous solution. The fluorine ion can also be adsorbed on the surface of Alumina by columbic attraction. The adsorbent with the clay only has the least number of fluoride removals.

Work was done on adsorption Isotherm and change in Free Energy. Here the model of Freundlich Isotherm was applied. The model is given mathematical as;

$Qe = K_f Ce1/n,$ (7)

Where 1/n and K_f are Freundlich constant which relate to adsorption intensity and capacity respectively.

The linear form would be as;

$lnqe = 1/n\ ln(Ce) + lnK_f$ (8)

Freundlich constants were determined from the graph of lnqe versus ln(Ce).It shows an increase in adsorption capacity,k_f, as the fluoride content of HA goes higher.

The free energy change in C-HA adsorbent was calculated using the relation;

$\Delta G = -RTlnK_o$ (9)

Where ΔG (kJ/mol) is the change in free energy, R (8.314/molK) is the universal gas constant, T is the absolute temperature and K_o is the thermodynamic distribution coefficient for the adsoption process.

The values obtained is presented in the table below

Adsorbent Type	Sintering Temperature (°C)	Freundlich isotherm parameters			
		K_f	1/n	R^2	

C-HA = 0:100	500	0.714	0.523	0.982
	600	0.657	0.524	0.987
	700	0.235	0.746	0.993
	800	0.219	0.742	0.956
	900	0.072	0.977	0.957
C-HA = 75:25	500	0.027	1.130	0.934
	600	0.032	1.103	0.983
	700	0.008	1.500	0.906
	800	0.012	1.398	0.972
	900	0.011	1.398	0.962
C-HA = 80:20	500	0.008	1.500	0.906
	600	0.030	1.120	0.937
	700	0.010	1.375	0.969
	800	0.009	1.439	0.939
	900	0.007	1.482	0.971
C-HA = 90:10	500	0.005	1.603	0.988

	600	0.010	1.398	0.995
	700	0.002	1.823	0.993
	800	0.003	1.637	0.999
	900	0.004	1.555	0.97
C-HA = 100:0	500	0.006	1.404	0.911
	600	0.003	1.542	0.864
	700	0.001	1.870	0.941
	800	0.002	1.723	0.96
	900	0.000	2.853	0.931

Freundlich Isotherm parameters and Gibbs free energy obtained for all adsorbent .(Yakub et al,2010.)

Table.7

Clay to HA Ratio	E.coli Removal (%)	E.coli Removal (LRV)	Initial Fluoride Concentration, C_o(mg/L)	Final Fluoride Concentration,* C_f(mg/L)	Initial pH	Final pH*
75-25			2.5	0.265 ± 0.043	6.332 ± 0.009	12.443 ± 0.127
			20	2.026 ± 1.144		11.493 ± 0.544
80-20			2.5	0.157 ± 0.015		12.199 ± 0.083
			20	2.333 ± 1.150		11.053 ± 0.531

Table 8. Proof-of-concept results using frustum-shaped C-HA filter. *Averaged over a cumulative volume of ~500mL (Yakub et al 2010)

The paper at the end was able to show that the biological and chemical contaminant in water can be eliminated by using a heterogeneous adsorbent in a process of co-sintering with defluoridating material like hydroxyapatite. The concept clearly indicates that C-HA based filter is also another potential improved method for point-of-used water purification technique for removing fluoride and micro-organisms.

2.2 PHYSICAL AND MECHANICAL PROPERTIES OF CERAMIC WATER FILTER

PHYSICAL PROPERTIES: The physical properties of ceramic water filters include ;the strength, density and the porosity .The non-availability of similar constituent of raw material across the world affects the flow of microstructure of ceramic water filter(4-8).The strength of ceramic water filter is define by the microstructural porosity and density(4,9).Also changing the composition of clay and plant by-product can affect the physical properties of the filter. Physical properties of ceramic water filter can therefore be seen as function of raw material composition that is used in manufacturing [2].

The porosity of ceramic filter can be defined by the volume fraction of sawdust or any other plant by-product or agricultural waste used in manufacturing. The mathematical relationship is expressed as Porosity(y) = pV +q, where p and q are the slope and intercept, and V is the volume fraction of agricultural waste.[2].The pore sizes of clay in the production of the filter can influence the structural integrity of the filter[9] .

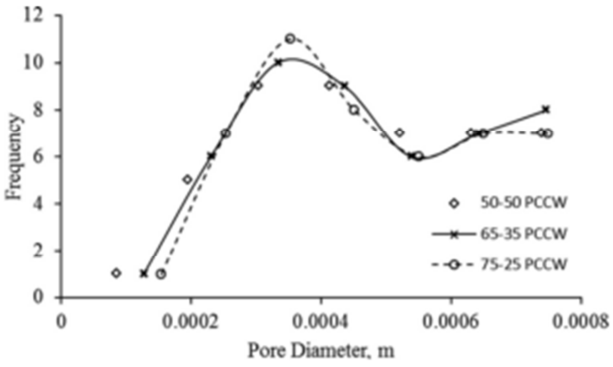

Fig. 4

Plappally,et al,2011)

Pore size distribution in porous clay ceramic ware samples.

The ceramic water filters which possess a bimodal pore size distribution tend to have high resistance to fracture. The porosity of filter can be measured by intrusion though difficult not damaging the material matrix, as closed pore porosity cannot measure with that method of intrusion. The effective porosity, n, is the open pore porosity which contributes to the passage of water through the filter.

Mathematically,

General Porosity = $\frac{Volume\ of\ Voids}{Total\ Volume\ of\ Sample}$ (10)

Effective Porosity,η, = $\frac{Open\ Porosity}{Total\ Volume\ of\ Porosity}$ (11)

Another method of estimating the porosity of porous material is using the Archimedes' Buoyancy principle. In this method a sample is weight in both air and distilled water, before being placed into boiling water to force water into the pores. The surface water is dried from the sample and this makes it to gain weight in air. The resulting differences make the calculation of Open- pore porosity [4].

Applying the principle, we have;

Volume of Sample V_s =$\frac{Weight\ in\ air - Weight\ in\ water}{density\ of\ water}$ (12)

Volume of open Porosity V_{op} =$\frac{Weight\ in\ boil\ water - weight\ in\ air}{Density\ of\ water}$ (13)

Porosity = $\frac{V_{op}}{V_{op}+V_s}$ (14)

2.2.1 Density of porous clay filter.

The average density of the various filter type manufactured is denoted as Y_d(g/cc).This is a function of volume fraction of sawdust(X).

Table 1 The density values for the PCCW materials discussed

	Density (g/cc)							
PCCWs	1	2	3	4	5	6	7	8
85-15	2.735	2.724	2.725	2.712	2.724	2.712	2.714	2.707
75-25	2.721	2.721	2.721	2.748	2.721	2.722	2.721	2.710
65-35	2.734	2.730	2.729	2.730	2.732	2.733	2.728	2.728
60-40	2.785	2.777	2.761	2.749	2.764	2.742	2.750	2.755
50-50	2.757	2.749	2.750	2.750	2.744	2.745	2.743	2.748

Table.9

Plappally et al 2011

Mathematically,

G= $G = \quad G_{k-1}X_k^{n_k} = mX_1^{n_1}X_2^{n_2} \ldots X_k^{n_k}$ (15)

g =g_i =$\ln G_i = \ln m + \sum_{i=1}^{k} n_i \ln X_i = m_o \sum_{i=1}^{k} n_i \ln X_i$ (16)

G = $\frac{X}{Y_d} = aX^b$ (17)

$\ln G = \ln a + b \ln X$ (18)

Where G is the response variable of the filter that its used to predicts the density and it is a function of sawdust, X with regression coefficient R^2= 99.99% and standard deviation, S =0.004993.

The response variable G, was found to be express as;

$G = e^{-0.978} \quad X^{0.991}$ (19)

This relation can be used to find the density of similar clay ceramic material that is manufacture with any quantity of plant material.

Eg. For a similar clay filter with volume fraction of sawdust of 30%

We have G =$e^{-0.978}(0.3)^{0.991} = 0.114 g/cm^3$

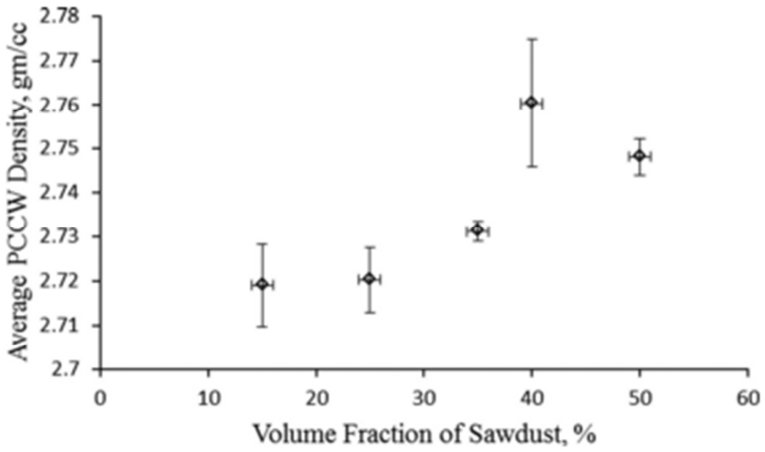

Plappally et al 2011.

Fig.5

2.3 Fundamental of fracture Mechanics

In 1920, the work of A.A.Griffith on the theoretical strength of material was accepted to be in the order of E/10, where E is the Young's Modulus for that particular material. This work was only considering elastic, brittle materials in which no plastic deformation do occurred. However, it was observed that the actual value of critical strength was as high as 1000 times less than the predicted value. This propels Griffith to further investigate the discrepancy.

He later discovered that there were many microscopic cracks in every material present at all times. These small cracks actually lowered the overall strength of the material because as a load is applied to these cracks, stress concentration comes to play in the material. In his work he considered an elastic body containing an internal crack of length 2c subjected to the external applied load at the boundary.

He tries to find the relation of the change of the free energy of the system with crack length as shown in the figure below

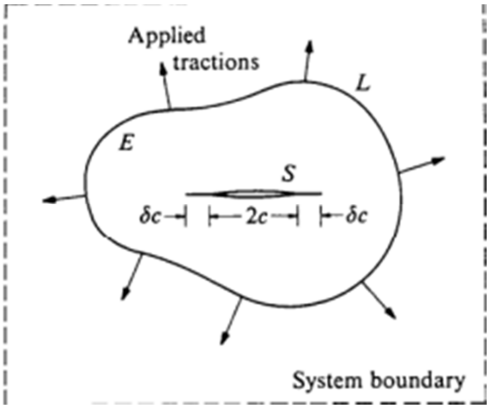

E is the elastic medium S, crack surface, L is applied load. For a static crack system, the total energy is the sum of three terms;

$$U = (\quad -W_L + U_E) + U_S$$

Thermodynamic equilibrium is attained by $\frac{du}{dc} = 0$

The work of Griffith provided the fundamental starting point for any fracture problem in which the operative forces could be considered to be conservative.

Considering a real situation of a narrow crack where b approach zero in a remote, uniform tensile stress field. The material is ideal linear elastic up fracture (like Glass).Under a constant applied force the mechanical energy of the body during crack formation can be calculated as;

$W_L = 2 \times \quad U_E$

Applying the solution of Inglis of stress and strain fields around sharp crack and integrating the strain energy over the whole domain gives ;(unit thickness)

$U_E = \pi c^2 \sigma_c^2 / E$ for plane stress (thin plate)

$U_E = \pi(1 - v^2) C^2 \sigma_L^2 / E$ for plain stress, thick plate

The surface energy of the crack system is

$U_s = 4c\gamma$ γ is the free energy per unit area. (Unit width)

The total system energy for plane stress case then becomes;

$$U = \pi C^2 \sigma_L^2 / E + 4C\gamma$$

Applying Griffith equilibrium condition $\frac{du}{dc} = 0$, we have the critical condition for fracture as;

$\sigma_L = \sqrt{[\frac{2E\gamma}{\pi c}]}$ Constant load for plane stress condition

$\sigma_L = \sqrt{[\frac{2E\gamma}{(1-V^2)\pi c}]}$ Plane strain condition at constant load

The plots for the mechanical energy, the surface energy and the total energy are shown in the figure below. It is seen that at equilibrium$\frac{du}{dc} = 0$, the system energy reaches a maximum ($\frac{d^2U}{dc^2} <$ 0), so the configuration is unstable. Which means if the applied stress exceeds the critical level, the crack is free to propagate spontaneously without limit [14 and 15].

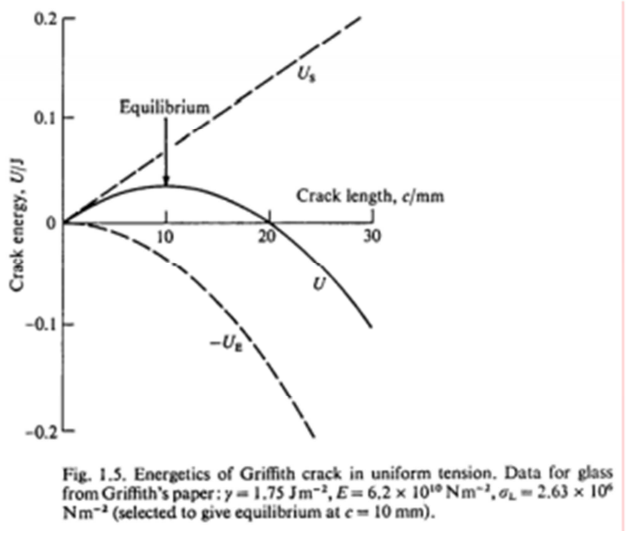

Fig. 1.5. Energetics of Griffith crack in uniform tension. Data for glass from Griffith's paper: $\gamma = 1.75\ \mathrm{J\,m^{-2}}$, $E = 6.2 \times 10^{10}\ \mathrm{N\,m^{-2}}$, $\sigma_L = 2.63 \times 10^{6}\ \mathrm{N\,m^{-2}}$ (selected to give equilibrium at $c = 10$ mm).

G.R.Irwin, in 1950, began to extend theory of Griffith to ductile materials. He determined that there was also certain energy from plastic deformation that had to be added to the strain energy originally considered by Griffith in order for the theory to work for ductile materials. Irwin in his work developed the concept of the strain energy release rate [17].

2.2.1 The stress intensity factor

While the energy- balance approach provides a great deal of insight to the fracture process, an alternative method that examines the stress state near the tip of a sharp crack directly has

proven more useful in engineering practice. There are three types of cracks, term as mode I, II and III as illustrated below in figure below.

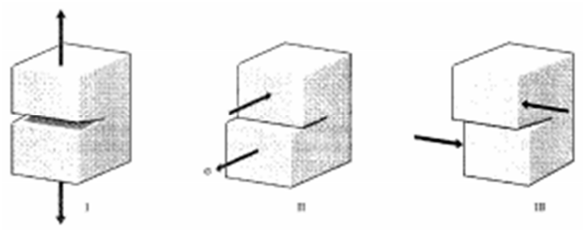

fig6

Mode I is a normal- opening mode and is the most destructive, while mod II and III are shear sliding modes. The crack tip stresses of mode I is given by

$$K_I = \alpha\sigma\sqrt{\pi a}$$

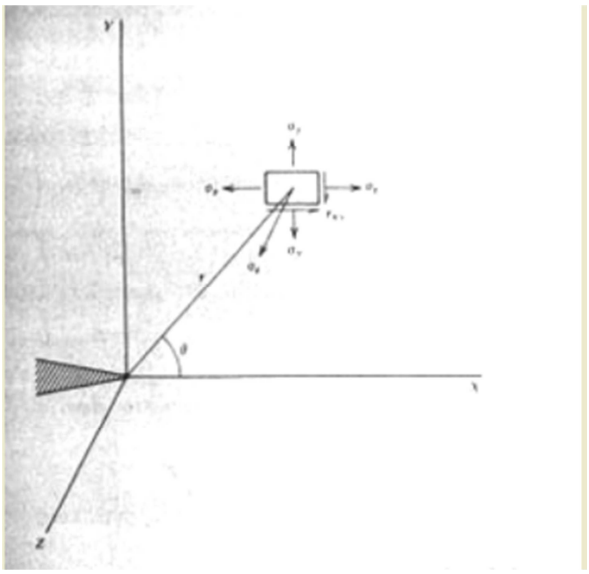

Distribution of stresses in vicinity of crack tip.

The stress field around the tip of crack under the linear elastic fracture mechanic from the figure above is as follows;

$$\sigma_y = \frac{K}{\sqrt{2\pi r}}\cos\frac{\theta}{2}\left(1+\sin\frac{\theta}{2}\sin\frac{3\theta}{2}\right) \qquad 1$$

$$\sigma_x = \frac{K}{\sqrt{2\pi r}}\cos\frac{\theta}{2}\left(1-\sin\frac{\theta}{2}\sin\frac{3\theta}{2}\right)$$

$$\tau_{xy} = \frac{K}{\sqrt{2\pi r}}\left(\sin\frac{\theta}{2}\cos\frac{\theta}{2}\cos\frac{3\theta}{2}\right)$$

The parameter K in the equation is a very important parameter known as the stress intensity factor.K_I is the stress intensity factor for mode I, similar relations is used for mode II and mode III.The relations show three factors that are taken together to depict the stress state near the crack tip: the denominator factor $(2\pi r)^{-1/2}$ shows the singular nature of the stress distribution: σ approaches infinity as the crack tip is approached with a $r^{-1/2}$ dependency. The K factor gives the overall intensity of the stress distribution, hence the name stress intensity factor. These stress intensity factors are used in design and analysis by arguing that the material can withstand crack tip stress up to a critical value of stress intensity, termed K_{ic}, beyond which the crack propagate rapidly. This critical stress intensity factor is then a measure of material toughness. The Failure stress σ_f is related to the crack length, a, and the fracture toughness by

$$\sigma_f = \frac{K_{Ic}}{\alpha\sqrt{\pi a}}$$

α is a geometrical parameter equal to 1 for edge cracks and generally on the order of unity for other situations .The energy release rate and the stress intensity factor are also related as illustrated below;

We know that;

$\sigma_f = \sqrt{\frac{EG_c}{\pi a}}$

So we have $\frac{K_{Ic}}{\alpha\sqrt{\pi a}} = \sqrt{\frac{EG_c}{\pi a}}$

This gives $K_{Ic}^2 = EG_c$

$K_{Ic}^2 = EG_c(1 - V^2)$ for plane strain condition.(18)

2.3 FINITE ELEMENT METHOD

Finite Element Analysis (FEA) was first introduced in 1943 by R. Courant, who applied the Ritz method of numerical analysis and minimization of variation calculus to obtain approximate solutions to vibration systems. At this age its application was limited since computers were expensive and owned by few organizations like the aeronautics, automotive, defense and nuclear industries. Today, with the rapid declined in the cost of computers, the application of FEA has increase in many areas of life [1].

Although analytical techniques are very important, the used of numerical methods to solve mathematical models of complex structures has become an essential ingredient in the designed

process. The finite element method has been the fundamental numerical procedure for the analysis of such models[2].

FEA consists of a computer model of a material or design that is stressed and analyzed for specific results. It is used to design new product and refined the existing ones. The FEA is based on idea of building a complicated object with simple ones or dividing the complicated object into small and manageable pieces.FEA can be applied in designed analysis, in computer simulation method in engineering as well as integrating it with CAD/CAM application. In terms of fracture, FEA most often involved the determination of stress intensity factors.

There are generally two types of analysis that are used in FEA:2-D modeling and 3-D modeling. The 2-D modeling analysis is simple, runs on normal computer and yield less accurate results. The 3-D modeling however, required a fast computer to run effectively and produces accurate results.

2.3.1 Types of engineering Analysis

Structural analysis. It involved both linear and non-linear models. The linear model is applied for simple parameters and assumes that the material does not undergo plasticity. The non-linear model, takes into account the plasticity of the material and that the stress in the material varies with the deformation of the material.

Vibrational analysis: this involved the test of material against random vibrations, impacts and shock. This may cause resonance and eventually lead to failure.

Fatigue analysis:this play a vital role in predicting the life time of a material or the effect of cyclic loading on the structure.

Heat Transfer analysis: it comes into play when one models the conductivity or thermal fluid dynamic of the material. This may be transient transfer or steady –state transfer.

Theory of finite element

2.3.2 GENERALIZATION OF FINITE ELEMENT

Galerkin-Weighted residual and variatioinal Methods

Given a function u, which satisfies a differential equaton

$$A(u) = \begin{pmatrix} A_1(U) \\ A_2(U) \\ . \\ . \\ . \end{pmatrix} = 0 \qquad (1)$$

In a domain $\Omega = \{volume, area, etc\}$

Boundary conditions;

$$B(u) = \begin{pmatrix} B_1(u) \\ B_2(u) \\ . \\ . \\ . \end{pmatrix} = 0 \qquad (2)$$

On the boundaries Γ of the domain.

The function can be scalar quantity or vector variables. Also the differentiation equation may be single or simultaneous and not necessary linear.

Let seek an approximation solution in the form

$$U = \sum_{i=1}^{n} Niai = \mathcal{N}a \qquad (3)$$

Ni are shape functions in term of independent variable x,y etc and all or most of the parameters ai are

What we have to note is that;

(a)the shape functions are defined locally for element or subdomains and

(b) the properties of discrete systems were recovered if the approximating equations were cast in an integral form.

We can now write the equation from which the unknown parameters ai in the integral form

$$\int_{\Omega} Gj(u)d\Omega + \int_{\Gamma} gj(u)dr = 0, \quad j = 1\ to\ n \qquad (4)$$

$$Gj\ and\ gj\ are\ known\ functions\ or\ operators.$$

The integrals above permit approximation to be obtained element by element and assemble to standard discrete systems. Since $Gj\ and gj$ are integrable, we have

$$\int_{\Omega} Gj\ d\Omega + \int_{\Gamma} gj\ dr = \sum_{e=1}^{m} (\int_{\Omega} Gj\ d\Omega + \int_{\Gamma} gjdr = 0 \qquad (5)$$

Where Ω^e is the domain of each element and Γ^e its part of the boundary

There are two methods of obtaining the approximation in such integral form; the weighted residuals (Galerkin method) and the variational functional.

If we assume that (1) and (2) are linear, then we can write

A(u) = L(u) + p =0 in Ω

B(u) = M(u) + t = 0 in Γ

By approximating (3), we have

Ka + f=0 with

$k_{ij} = \sum k_{ij}^e$ $f_i = \sum_{e=1}^{m} f_i^e$

2.3.3 The Weighted Residual Method

For the set of differential equations in (1) to be zero at each point of the domain Ω then we have to get

$$\int_{\Omega} V^T A(u) d\Omega \equiv \int_{\Omega} [V_1 A_1 + V_2 A_2(u) + \cdots] d\Omega \equiv 0 \qquad (6)$$

Where $V = \begin{Bmatrix} V_1 \\ V_2 \\ . \\ . \\ . \end{Bmatrix}$ is a set of functions equal in number to the number of equations involved

2.3.4 Variational Principles

It specifies a scalar quantity (functional)Π, which is defined by an integral form

$$\Pi = \int_{\Omega} F(u, \frac{du}{dx}, \dots) d\Omega + \int_{\Gamma} E(u, \frac{du}{dx}, \dots) d\Gamma \qquad (7)$$

In which u is the unknown function and F and E are specified differential equations.

2.3.5 Method of calculating stresses using finite element

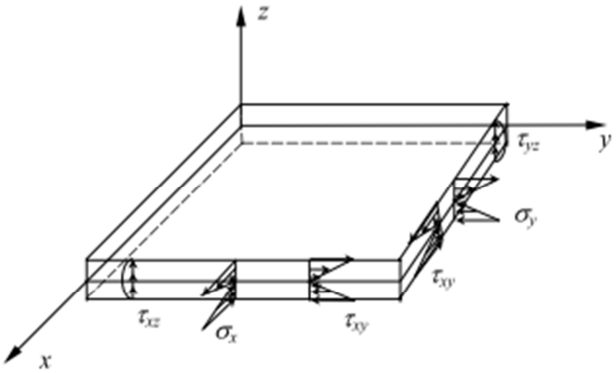

Fig.8

From the diagram above we can obtained the relationship between forces and stresses as follows;

Bending moments per unit length:

$M_x = \int_{-t/2}^{t/2} \sigma_x \, z dz,$

$M_y = \int_{-t/2}^{t/2} \sigma_y z dz$

The twisting moment per unit length:

$M_{xy} = \int_{-t/2}^{t/2} \tau_{xy} z dz,$

Shearing forces,

$Q_x = \int_{-t/2}^{t/2} \tau_{xz} dz$,

$Q_y = \int_{-t/2}^{t/2} \tau_{yz}\, dz$

The maximum bending stresses are;

$(\sigma_x)_{max} = \pm \frac{6M_x}{t^2}$ and $(\sigma_y)_{max} = \pm \frac{6M_x}{t^2}$

This are always obtained at $z = \pm t^2/2$ with no bending stresses at the mid surface.

Considering the plate theory, we assumed here that a straight line along the normal to the mid surface remains straight and normal to the deflected mid surface after loading, that is, there is no transverse shear deformation:

$$\gamma_{xz} = \gamma_{yz} = 0$$

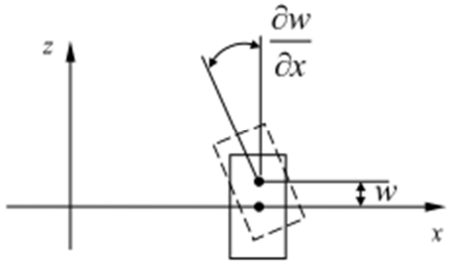

Fig.9

Displacement along x,y deflection from the diagram is;

$U = -z\frac{dw}{dx}$, $V = -z\frac{dw}{dy}$

This yields the strain equations as;

$$\varepsilon_x = -z\frac{\partial^2 w}{\partial x^2},\ \varepsilon_y = -z\frac{\partial^2 w}{\partial y^2},\quad \tau_{xy} = -2z\frac{\partial^2 w}{\partial x \partial y}$$

We note here that there is no stretch of the mid surface due to the deflection (bending) of the plate.

In a plane stress condition, we have;

$$\begin{bmatrix}\sigma_x\\ \sigma_y\\ \tau_{xy}\end{bmatrix} = \frac{E}{1-v^2}\begin{bmatrix}1 & v & 0\\ v & 1 & 0\\ 0 & 0 & 1-v/2\end{bmatrix}\begin{bmatrix}\varepsilon_x\\ \varepsilon_y\\ \tau_{xy}\end{bmatrix} \qquad (8)$$

2.3.6 Methods of calculating the crack driving forces using Finite element Method

2.3.6.1 J-Integral

The J-integral is a contour integral characterizing the strain energy release rate for an elastic non-linear material. The stress field is related to the strain energy density as:

$$\sigma_{ij} = \frac{\partial w}{\varepsilon_{ij}}$$

From the definition of potential energy along the contour, Rice defined an integral independent of the integration contour Γ around the cracks tips as:

$$J = \oint_\Gamma (w\,dy - T\frac{\partial u}{\partial x}ds) \qquad (9)$$

Where w is the strain energy density per unit volume is the traction vector (T=σ_n).U is the displacement vector and y is the direction perpendicular to the crack line. For linear or non-linear elastic materials,the strain energy release rate is equal to the energy release rate along

the a contour at crack tip vicinity (J =G); this parameter is related ti the stress intensity factor as G = K^2/E in the plane stress or G= $k^2/E(1-V^2)$ in plain strain.

K = $[GE(1-V^2)]^{1/2}$ for plane strain

K =$[GE]^{1/2}$ for plane stress.

2.3.6.2 Virtual crack closure Technique

This method also used the idea of energetic assumption. The virtual crack closure Technique (VCCT) is based on energy release rate when the crack grows with an infinitesimal increment. It is based on the calculation of the strain energy release rate, using the energy variation when an extension of the crack length is imposed:

$$G = \frac{\partial u}{\partial a} = \frac{U_{a+\Delta a} - U_a}{\Delta a} \qquad (10)$$

This approached was introduced by Rybicki and Kanninen in 1977,[16];howerver it requires two finite element analysis in order to calculate the strain energy release rate for specific crack length. In addition to the earlier assumption, it is also assumed that the crack tip are not significantly altered when it extends by an increment Δa, from a crack length a+Δa to a length a + 2Δa.This suggest that when the displacement of a region close to the tip, is at specific node, are approximately the same as the displacements at the same location when the tip is at the previous node.

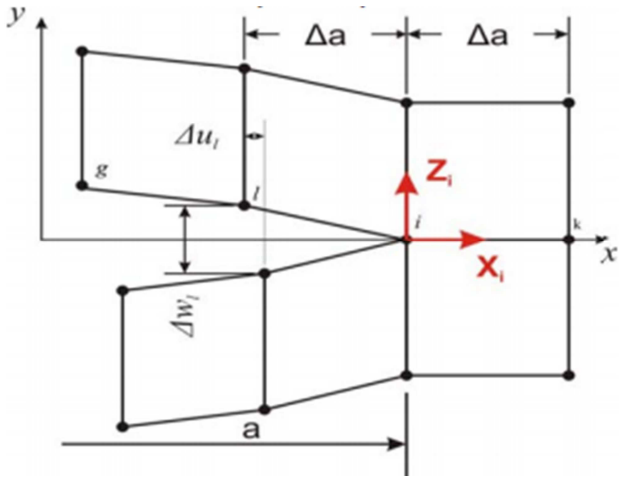

Fig.10

This is a modified virtual crack closure technique notation

The energy changes ΔE required to closed the crack along a distance Δa is given as

$$\Delta E = \frac{1}{2}(X_{i.} . \Delta U_i + Z_i . \Delta w_i)$$

Where $X_{i.}$ And $Z_i.$ are the nodal forces at point I and ΔU_i and Δw_i are the node I displacement

Therefore the information required for the calculation of the energy variation is obtained from a single finite element analysis. Having getting the energy variation, the energy release rate is determined as;

$$G = \frac{\Delta E}{\Delta A} = \frac{\Delta E}{\Delta a.b}$$

Where . ΔA is the surface area created by a crack propagation of Δa; in the case of plates with a thickness b,the area is Δa .b.The calculation of the strain energy release rates for each mode is made using the displacement and nodal forces corresponding to the strain energy of that mode.

$G_1 = -\frac{1}{2.\Delta a} Zi.\Delta w_i$

$G_{11} = -\frac{1}{2.\Delta a} X_i \Delta U_i$

If the finite element model was built using other types of elements of solid or plate element with 8 nodes, the strain energy release rate equation must be modified in order to take into account the effects of the other reaction forces [14].

CHAPTER THREE

The application of finite element method (FEM)

3.0 Modeling of Ceramic Water Filter Shapes Using Abaqus Software.

3.1 Finite Analysis Tool-ABAQUS

ABAQUS is a multi-purpose finite element method tool with a group of simulation programs, has the ability of modeling solids and structures under applied loading. Its capable of solving problems of simple structural form to a more complex nonlinear analysis.ABAQUS has a large library of elements where any type of geometry can be modeled. The application of ABAQUS has a much broader range of application many other different areas like heat transfer, mass diffusion, coupled thermal- electrical analysis, acoustics, soil mechanics, piezoelectric analysis, fracture mechanics, and simulations involving manufacturing processes(ABAQUS 6.9 student version Online Decumenttation,ABAQUS.).

Abaqus consists of two main analysis products ,Abaqus/Standard and Abaqus/Explicit. Abaqus/Standard solves implicit system of equations at each solution increment while Abaqus/Explicit uses an explicit dynamic finite element formulation and marches a solution forward through time in small time increments without solving a coupled system of equations at each increment.

Abaqus analysis has three stages; preprocessing, Simulation and postprocessing.These are joined together by files.

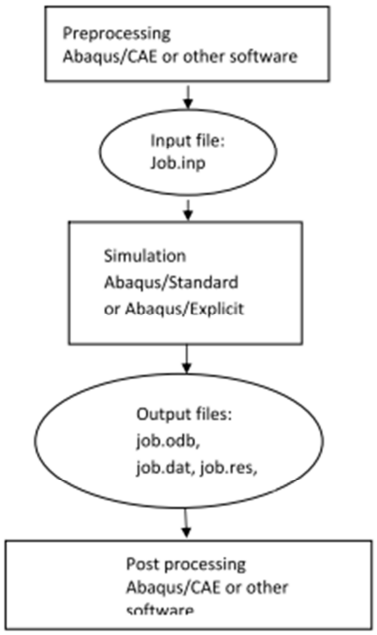

Fig.11

Preprocessing is the stage where the model of the physical problem is defined in the input file. This input file can be created using Abaqus/CAE.Simulation is the point in which Abaqus/Standard or Abaqus/Explicit solves the numerical problem that is defined in the model. At this time the output files are ready for post processing. Depending on how complex the problem is and the power of the computer being used is, it takes from seconds to hours to complete the analysis. Using the visualization module the results can be displayed with different contour plots animations, deformed shape plots and XY plots.

The required input for the ABAQUS finite element analysis comprised the model geometry, material properties, loading conditions, and an initial crack configuration. The general ABAQUS modules are shown in the figure

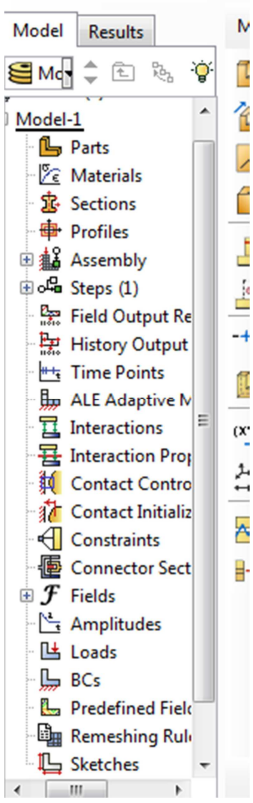

ABAQUS /CAE modules 6.9.

A description of the steps taken to perform the model of the shapes and the calculation of stress distribution using ABAQUS were as follows:

a. Create a two-dimensional shell model of the shape in the ABAQUS/CAE Part module.
b. Define material properties for the shapes in the Property module, including density, modulus of elasticity, and Poisson's ratio.
c. Create the sections of the geometry.
d. Create an assembly of the part in the Assembly module.
e. Create the mesh of the shell elements in the Mesh module

f. Create steps for the analysis in the step module

g. Apply boundary conditions and loadings in the generated input file, this consist of set of keywords defining the geometry, material properties and meshing of the entity

h. Create field output request

i. When all the keywords are defined, submit the input file to the job module to solve the analysis.

j. In post-processing, interpret the output in the Visualization module, including standard stresses, strain, and thickness variation.

Components of Abaqus Analysis model

Basically, analysis in Abaqus is made up of discrete geometry, element section properties material data loads and boundary conditions, analysis type and output requests.

DISCRETE GEOMETRY: The geometry is modeled using finite element and nodes. Each element in the modeled represents a discrete potion of the strucrure.They are linked to one another by nodes. The combination of these element and the nodes are called mesh of the modeled.

ELEMENT SECTION PROPERTIES; Abaqus has wide range of elements in its library that can be used for structural applications. The name of the elements identifies the element

group, formulation, number of nodes, and the type of integration. All elements are therefore referring to a section property definition. It also provides additional data needed to define geometry of element and identifies the associated material property.

MATERIAL DATA: All material data for an element must be indicated. These account for the validity of Abaqus simulation of any material.

Boundary conditions and loads: When loads are applied the material is distorted and therefore creating stress. Loads that are used in Abaqus include:

Concentrated loads

Pressure loads

Distributed tractions on the surfaces

Distributed edge loads and moments on shells edges

Body forces, like gravity and

Thermal loads.

Boundary conditions are applied to restrict the motion of the portion of interest in the model. That the needed to be fixed. This portion is assigned zero displacement.

Analysis type:Abaqus can carry out many different types of simulations which include static, dynamic ,seismic, and quasi-static

Output requests: An abaqus simulation can generate a large amount of output. These can be limited by creating a report in the field output request to that required for interpreting the results of interest.

3.2 Modeling of filter geometry

As mention earlier, that this work is to come out with optimum choice of filter geometry to be used as water filter geometry. Three shapes were considered. These are the cylindrical base shape (circle) ,the rectangular base shape and the frustum shape. During the loading process a simple hydraulic press method was used. Using the simple pressure equation,

Pressure= density x gravity x height

The concentrated force was calculated using the relation,

Force = density of water x gravity x volume.

A constant volume and height were assumed for all the shapes. The properties used is presented in the table

Properties	Values
Density	2.3 g/cm^3
Young's Modulus	15 x 10^{6}Nm
Poison's ratio	0.33
Pressure	2548 Pa
Concentrated force	9810N

Table. 10

Due to symmetric nature of filter geometry, symmetry was model instead of the full geometry.

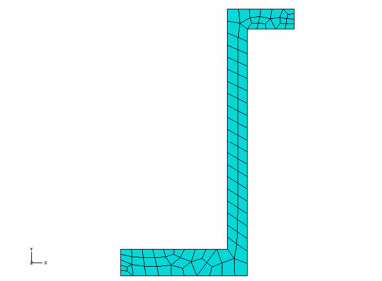

Rectangular base shape

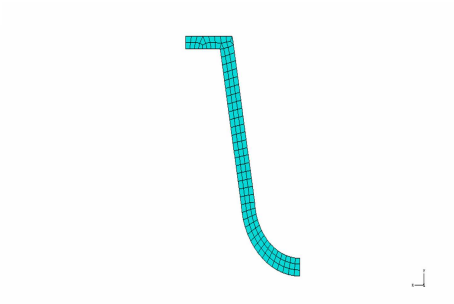

Cylindrical base shape

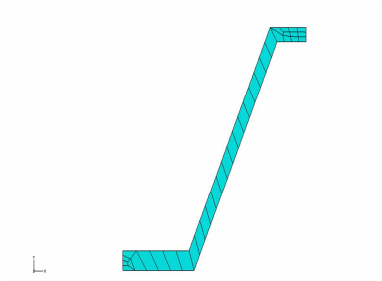

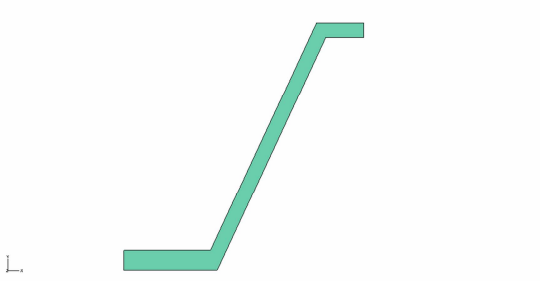

Frustrum shape

They were meshed and the stress distribution of the various shape were as follows.

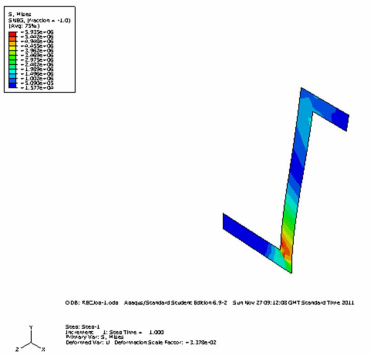

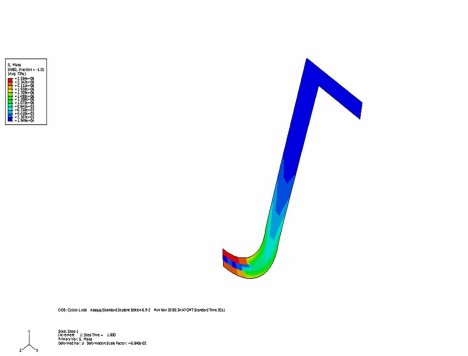

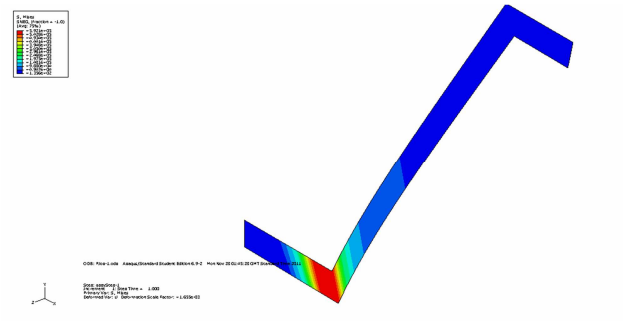

The thickness of each geometry was varied from 0.1mm to 0.4mm and at each thickness, the maximum principal stresses and the Von Mises stresses were recorded. The data is shown at the supplemtary data.

A graph of thickness versus maximum Principal stresses was plotted in order to compare the variation of the stresses with respect to changes in thickness.

Fig.12

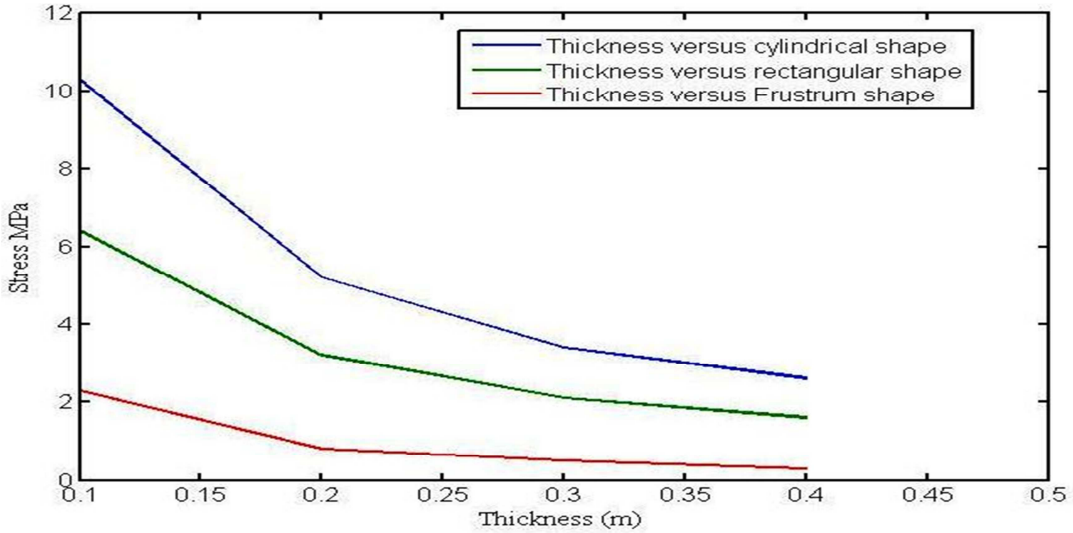

3.3 CRACK MODELING

Cracks were inserted at the corner of the geometry in order to determine the resistance abilities of the various filters. The crack lengths were varied from 0.1mm to 0.7mm with an increment of 0.2mm.At each crack length J-integral value was calculated. A graph of

J-.integral which is the energy release rate as described earlier was plotted versus crack length.

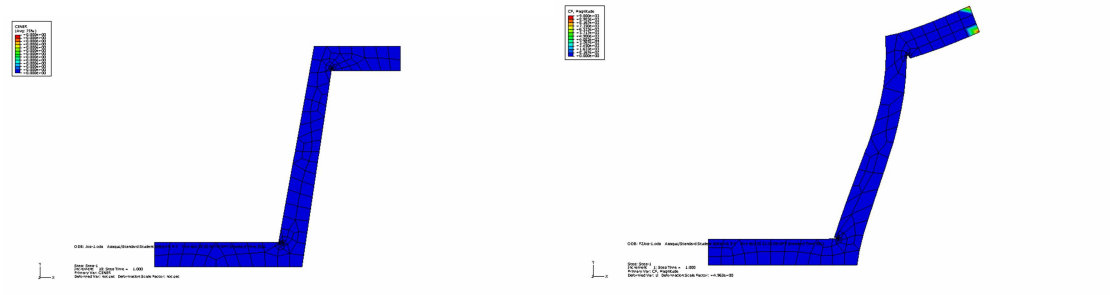

Frustum shape with crack.

The rest are presented at the last page of the report.

Fig.13

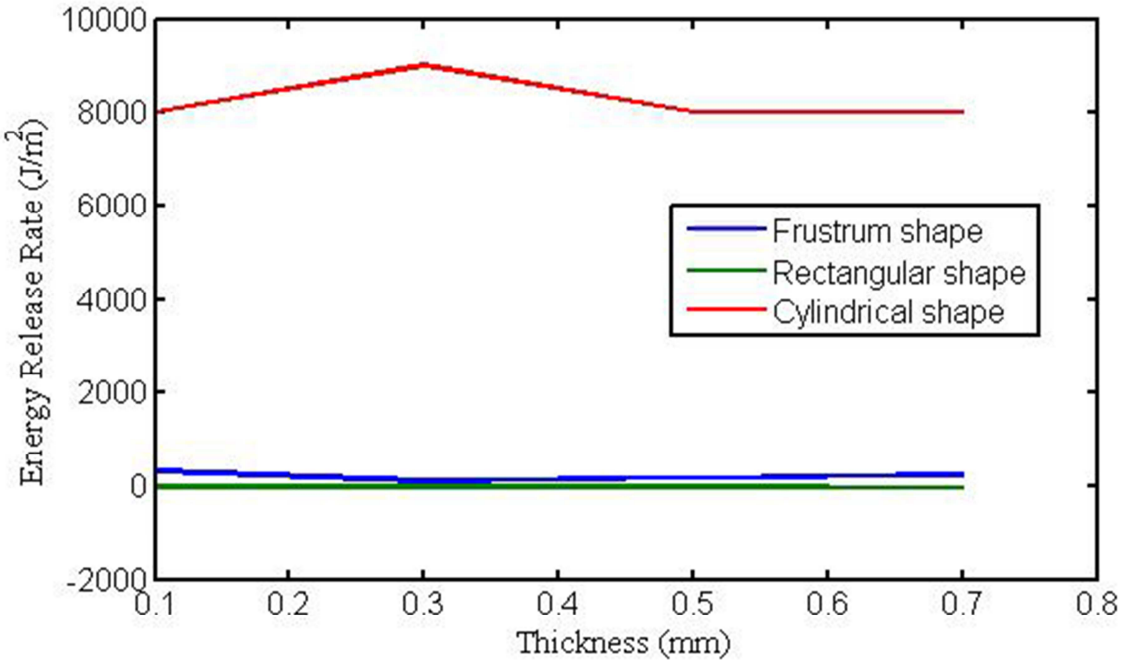

From the relation

$K = [GE(1-V^2)]^{1/2}$ for plane strain

$K = [GE]^{1/2}$ for plane stress.

The crack driving forces were calculated .Plane stress condition was assumed. A graph of crack driving forces versus crack length was plotted.

Fig.14

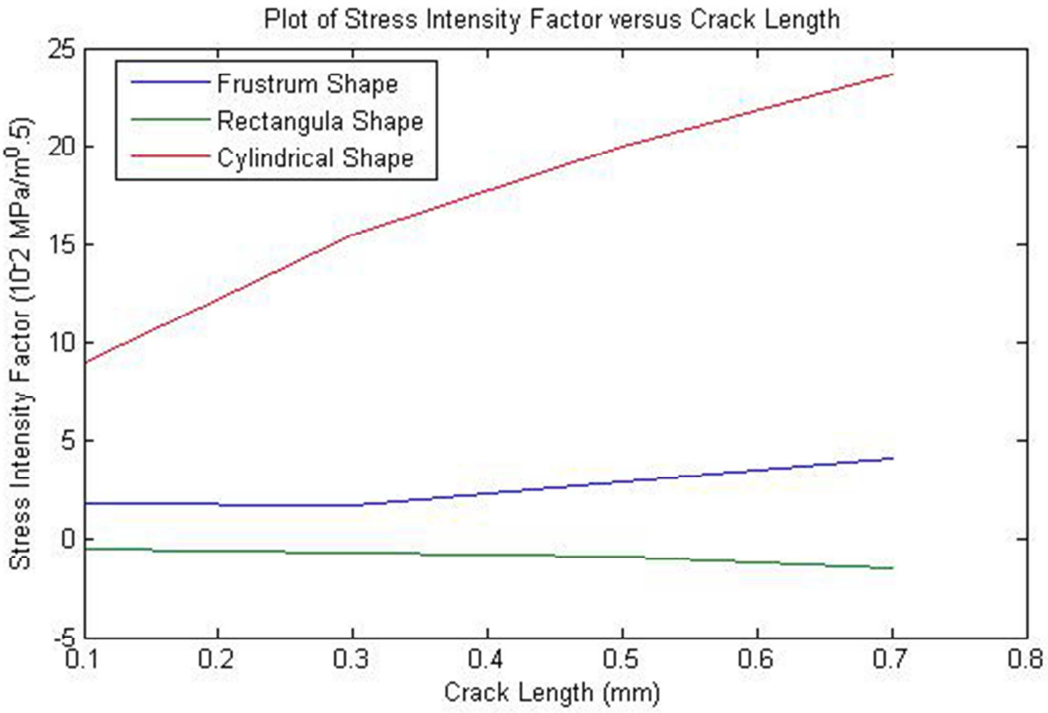

3.4 Cantilevered Support

The effect of Cantilevered support was also investigated for each of the three filters. Three elements were selected for each and plotted. The graphs are presented as;

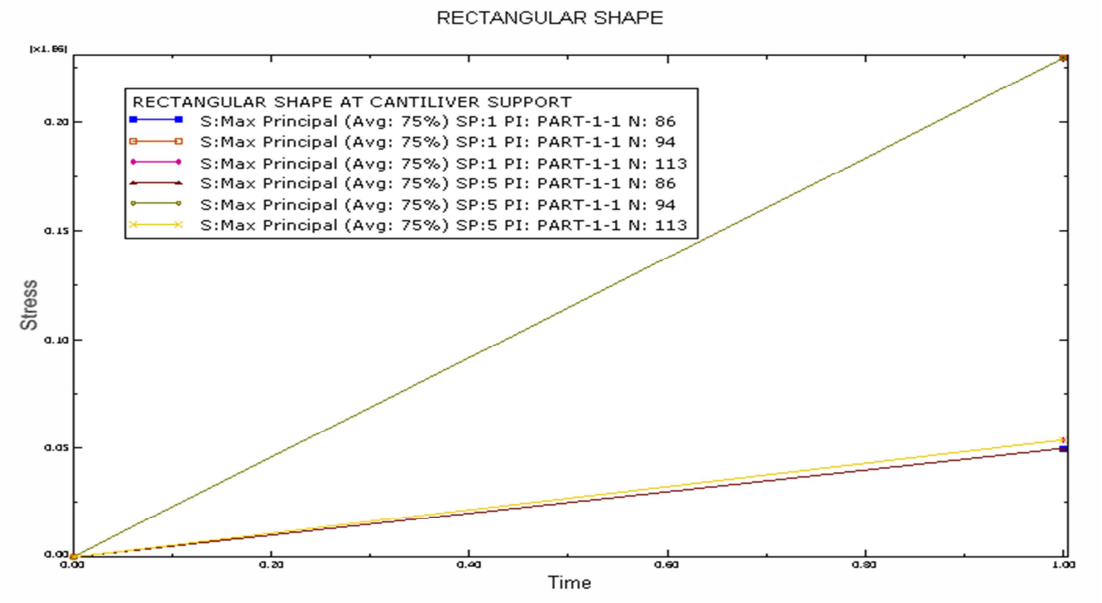
RECTANGULAR SHAPE
[x1.E5]
RECTANGULAR SHAPE AT CANTILIVER SUPPORT
S:Max Principal (Avg: 75%) SP:1 PI: PART-1-1 N: 86
S:Max Principal (Avg: 75%) SP:1 PI: PART-1-1 N: 94
S:Max Principal (Avg: 75%) SP:1 PI: PART-1-1 N: 113
S:Max Principal (Avg: 75%) SP:5 PI: PART-1-1 N: 86
S:Max Principal (Avg: 75%) SP:5 PI: PART-1-1 N: 94
S:Max Principal (Avg: 75%) SP:5 PI: PART-1-1 N: 113
Stress
Time

fig.15

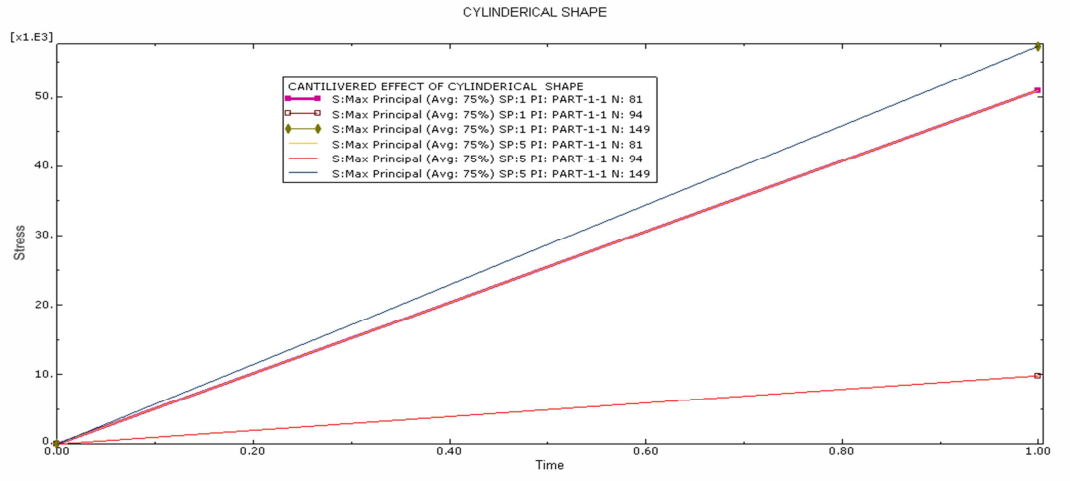
CYLINDERICAL SHAPE
[x1.E3]
CANTILIVERED EFFECT OF CYLINDERICAL SHAPE
S:Max Principal (Avg: 75%) SP:1 PI: PART-1-1 N: 81
S:Max Principal (Avg: 75%) SP:1 PI: PART-1-1 N: 94
S:Max Principal (Avg: 75%) SP:1 PI: PART-1-1 N: 149
S:Max Principal (Avg: 75%) SP:5 PI: PART-1-1 N: 81
S:Max Principal (Avg: 75%) SP:5 PI: PART-1-1 N: 94
S:Max Principal (Avg: 75%) SP:5 PI: PART-1-1 N: 149
Stress
Time

fig.16

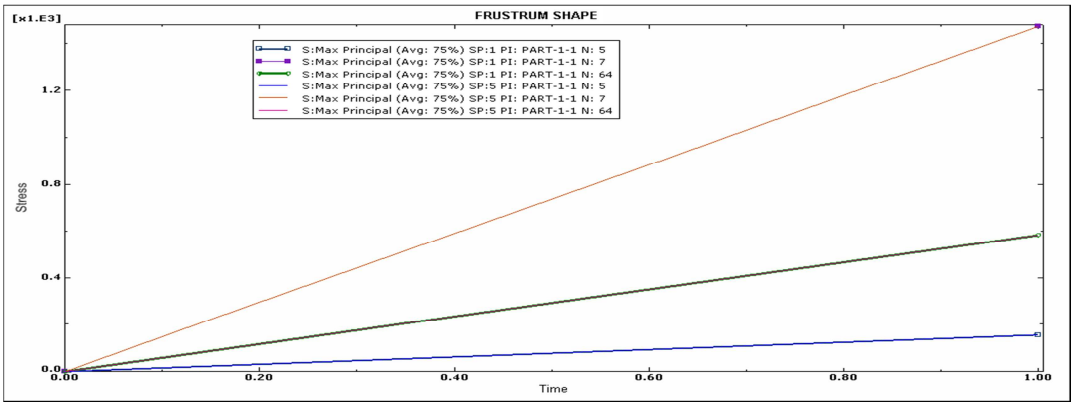
FRUSTRUM SHAPE
[×1.E3]
S:Max Principal (Avg: 75%) SP:1 PI: PART-1-1 N: 5
S:Max Principal (Avg: 75%) SP:1 PI: PART-1-1 N: 7
S:Max Principal (Avg: 75%) SP:1 PI: PART-1-1 N: 64
S:Max Principal (Avg: 75%) SP:5 PI: PART-1-1 N: 5
S:Max Principal (Avg: 75%) SP:5 PI: PART-1-1 N: 7
S:Max Principal (Avg: 75%) SP:5 PI: PART-1-1 N: 64
Stress
1.2
0.8
0.4
0.0
0.00
0.20
0.40
0.60
0.80
1.00
Time
fig.17

CHAPTER FOUR

4.0 DISCUSSIONS OF THE RESULTS.

From the simple gradient relationship, Q=H/T, where H is the height of the element T is the thickness of the element and Q is the flow rate .This implied that when thickness of the element is increase the flow rate reduces. Therefore element thickness must be kept as small as possible in order to obtain a maximum flow rate of the filter. Also, when the flow rate goes high the hydraulic conductivity of the element increases which suggest high porosity of the filter.

Mechanically, as observed from the graph, the smaller the thickness the larger the Principal maximum stress of the filter. The effect of this is extended to the crack driving forces of the element.

The crack driving forces is also seen to be a function of loading, crack length and the structural geometry. Also the flaw changes with the thickness of the element until that thickness exceeds some critical dimension. Once the thickness exceeds the critical dimension the value of K_1 becomes relatively constant and this is the K_{1c} of the element. This is a true material property of the element. At this point unstable fracture occurs.

The parameter, J-integral can also be used to characterize a material. However, the toughness data produced by this parameter will be dependent on the thickness of the product and will not be a true material property.

From the previous work the fracture toughness of filters is in the range of 0.6MPam$^{1/2}$ to 0.4MPam$^{1/2}$.This is comparable to what is display in this work, which suggest that frustum shape is the optimum geometry with fracture toughness of 0.3MPam$^{1/2}$ to 0.5MPam$^{1/2}$.

On the aspect of the cantilevered support, the cylindrical shape displayed the highest Maximum principal stress and frustum shape is the lowest. This show that at the cantilevered of frustum shape need to be thicken in order to support is resistance to fracture.

CHAPTER FIVE

5.0 CONCLUSION AND RECOMMENDATION

From the results of the thickness graph and the stress intensity factor, it can be concluded that the frustum shape is the optimum choice of geometry for ceramic water filter. Also the thickness of an element greatly affect flow rate of filter. Fracture and rupturing are irreversible processes at stress concentration which determine toughness of an element of the filter.

5.1 Future Work

A more thorough investigation into the effects of stress distribution and thickness of the geometry of ceramic water filter could be undertaken in order to gain greater understanding of the relationship among the stress, thickness and crack length on the geometry of the filter.

Further investigation on the effect of bumping and impulse could be undertaken in order to account for the maximum impulse before fracturing during transportation. There is the need to scale –up ceramic water filter by creating a reservoir of tank to filter water to supply large number of people. The critical thickness for the reservoir could be investigated using the Abaqus/Explicit which could perform finite element analysis on brittle material.

REFERENCE

1) United Nations.(september2002)"World Summit on Sustainable Development-Key outcome fo the summit"Johannesburg,SouthAfrica,August26toSeptember4,2003.
2) Website:<http:www.johannesburgsumit.org>,now on www.un.org
3) World health organization.("Global water supply and sanitation Assessment 2000 Report".Genva,Switzerland.
4) World Health organization(August 28,2002)"Water,sanitation and Hygiene Links to Health-Facts and Figures" file.
5) United States Environmental Protection Agency.(April 1987)"Guide Standard and Protocol for Testing Microbiological Water Purifiers". Registration Division, office of Pesticide Program,Criteria and Standard Division, Office of Drinking water.
6) United States Environmental Protection Agency. "National Secondary Drinking Wtaer regulations.
7) Du Preez,M,Cornroy,R.M.Wright,J.A.Moyo,S.Potgieter,N.Gundry, S.W.,2008" Used of ceramic water filtration in the prevention of Diarrheal Disease:A Redomized controlled trial in Rural South Africa and Zimbabwe"Am,J.Trop,Med.Hyg,79(5),
8) Plappally,A.Chen.H.,Ayinde,W.,Alayande.S.,UsoroA.,Friedman,K.,Dare.E.,Ogunyale,T.,Yakub.I.,Leftwich

9) M.,Malatesta.K.,Rivera.R.,Brown.L.,Soboyejo,A. and Soboyejo.W.,2011,"A field Study on the use of clay ceramic water filters and influences on the General health in Nigeria.website:www.asciencejournal.net/asj/index.pbp/HBPH/article/view/109.

10) Plappally,A.K. 2010,"theoretical and Empirical Modeling of flow, strength, leaching and Mirco-structural characteristics of V shaped Porous ceramic water filters"Doctoral Dissertation Publication no. 3428662,The Ohio State University,Columbus,OH.

11) Nandi,B.K.,Uppaluri.R., and Purkait,M.K.,2008,"Preparation and characterization of low cost ceramic membranes for micro-filtration application".

12) .Brown and Soboyejo. M, 2006, Independent Appraisal of ceramic water filtration intervention in Cambodia, "Final report university of North Carolina of public Health Department of Environmental Sciences and Engineering, Submitted to UNICEF.

13) Roberts, m.2004,"Field Test of Silver Impregnated ceramic water filter, Vientiane, lao PDR: 30thWEDC International conference.

14) CAWST,2009,water hygiene and sanitation, January 2009.

15) www.sv.vt.edu/classes/MSE2094_NoteBook/97ClassProj/num/midkiff/theory.html

16) Yijun Liu,CSE Research Laboratory mechanical Engineering Department university of Cincinnati,Cincinnati,OH45221-0072,USA.

17) Tabbal, Georges.(May2003) "Technical and Social Evaluation of three Arsenic Removal Technologies". Master of Engineering thesis. Department of civil and Environmental Engineering,Massahusetts Institute of Technology,Cambridge,MA

18. Development of a ceramic water filter for Nepal, by Robert Dies, University of British Columbia,Canada,2001.
19. Physical properties of porous Clay Ceramic-Ware by A.K.Plappally et al,2011.
20. A field study on the use of clay ceramic water filters and Influences on the general health of in Nigeria, Anand and Plappally et al, 2011.
21. http://ceae.colorado.edu/mc-edc/pdf/scotland%20study.pdf
22. Soboyejo and malatesta lecture notes on Biomedical and Innovation,AUST-Abuja,Nigeria
23. .(oyandel-craver-and-smith,2008)
24. Brown,J; Sobsey,M.Ceramic media amended with metal oxide for the capture of viruses in drinking water. Environ.Technol.2009
25. Ruan,H;frost,R;Kloprogge;J;Duong,L.Infrared spectroscopy of goethite dehydroxylation
    a. Microscopy of in situ study of the thermal transformation of goethite to hematite.
26. Brito,M.E.2007,Development in porous, Biological and Geopolymer ceramic
27. O.C Zienkiewicz and R.L.Taylor,Finite Element method
28. J.NReddy,An introduction To Finite Element Method
29. Finite Element Modeling for stress Analysis
30.) B. Lawn and Shaw, “Fracture of Brittle Solids”, (1975, 1993)
31. A. E. Maugin, “The Thermomechanics of Plasticity and Fracture”, (1992)
32. www.sv.vt.edu/classes/MSE2094

33. 17. M.L.Bucalem and K.J.Bathe,Finite of finite element analysis of shell structures,Archives of computational methods in Engineering
34. T.R.Bathe , Finite Element Procedures(Prentice hall,Englewood Cliffs,NJ,2002.
35. STRESS INTENSITY FACTORS BY NUMERICAL EVALUATION IN CRACKED STRUCTURES S.M.O. TAVARES*, P.M.G.P. MOREIRA*, S.D. PASTRAMA**, P.M.S.T. CASTRO*]
36. E.F. Rybicki and M.F.Kanninen,Finite element calculation of stress intensity factors by modified crack closure integral, Engineering Fracture Mechanics
37. R.Krueger.the virtual crack closure technique;history approach and applications
38. http://www.parnell-eng.com/presentations/FractureIntro9_pics_noLogo.pdf
39. http://ocw.mit.edu/courses/materials-science-and-engineering/3-11-mechanics-of-materials-fall-1999/modules/frac.pdf
40.

Supplementary Data.

Planer shape

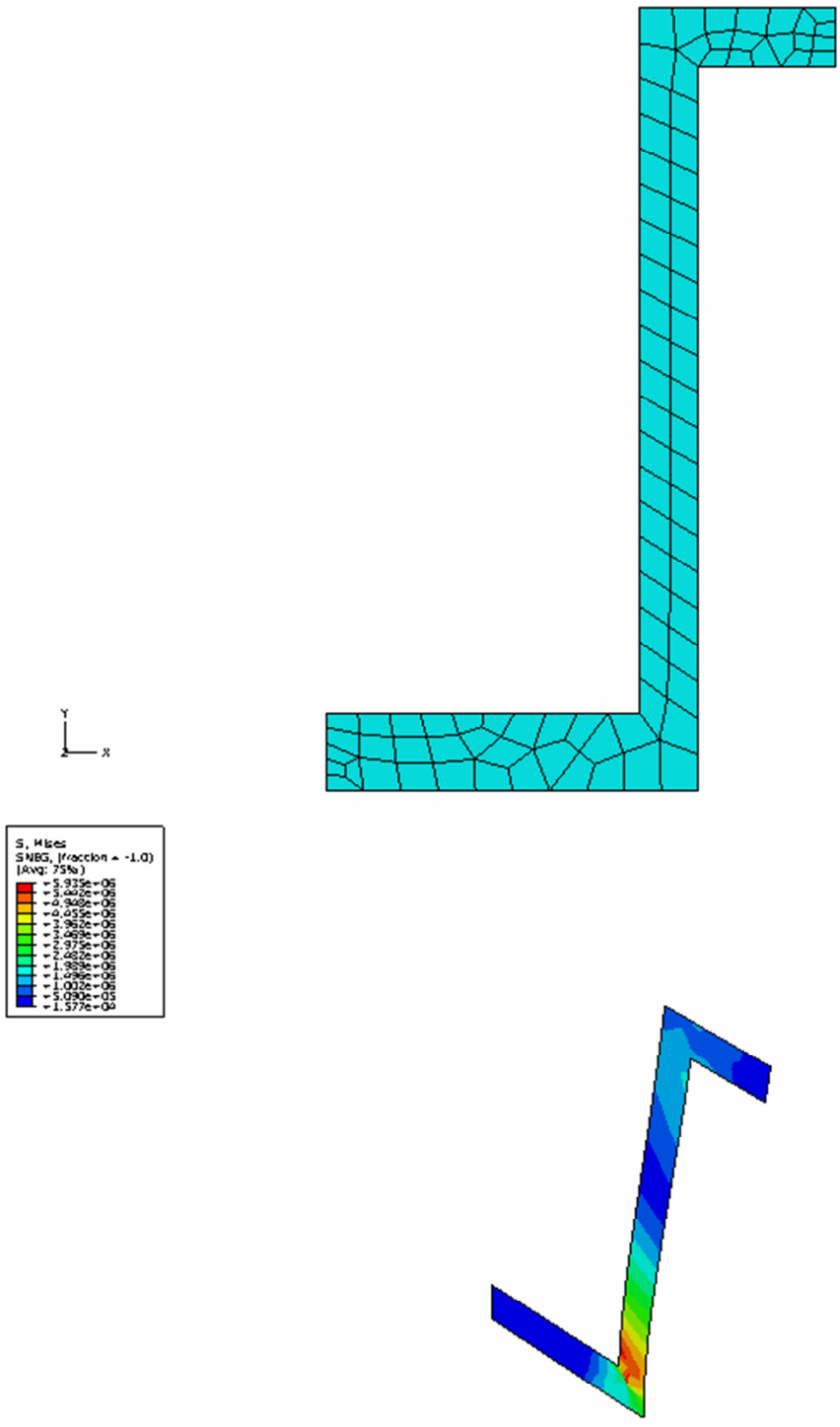
Y
X
S, Mises
SNBG, (fraction = -1.0)
(Avg: 75%)
+5.935e+06
+5.442e+06
+4.948e+06
+4.455e+06
+3.962e+06
+3.469e+06
+2.975e+06
+2.482e+06
+1.989e+06
+1.496e+06
+1.002e+06
+5.090e+05
+1.577e+04
ODB: RBCJoa-1.odb Abaqus/Standard Student Edition 6.9-2 Sun Nov 27 09:12:08 GMT Standard Time 2011
Y
Z
X
Step: Step-1
Increment 1: Step Time = 1.000
Primary Var: S, Mises
Deformed Var: U Deformation Scale Factor: +3.378e-02

	Mises(loc1)	Mises(loc2)	S.Maxi(loc1)	S.MaxL2
Minimum	14.4151E+03	14.4151E+03	0.	0.
At Element	1	1	77	77
Int Pt	1	1	1	1
Maximum	5.93486E+06	5.93486E+06	6.44187E+06	6.44187E+06
At Element	36	36	36	36
Int Pt	1	1	1	1
Total	101.051E+06	101.051E+06	58.6386E+06	58.6386E+06

t=0.1

Minimum	7.45018E+03	7.45018E+03	0.	0.
At Element	1	1	79	79
Int Pt	1	1	1	1
Maximum	2.92101E+06	2.92101E+06	3.17684E+06	3.17684E+06
At Element	36	36	36	36
Int Pt	1	1	1	1
Total	49.9490E+06	49.9490E+06	28.9740E+06	28.9740E+06

t=0.2

Minimum	5.03227E+03	5.03227E+03	0.	0.
At Element	1	1	79	79
Int Pt	1	1	1	1
Maximum	1.92354E+06	1.92354E+06	2.09391E+06	2.09391E+06
At Element	36	36	36	36
Int Pt	1	1	1	1
Total	33.0304E+06	33.0304E+06	19.1605E+06	19.1605E+06

t=0.3

Minimum	3.79381E+03	3.79381E+03	0.	0.
At Element	1	1	79	79
Int Pt	1	1	1	1
Maximum	1.43115E+06	1.43115E+06	1.55858E+06	1.55858E+06
At Element	36	36	36	36
Int Pt	1	1	1	1
Total	24.6471E+06	24.6471E+06	14.3013E+06	14.3013E+06

t=0.4

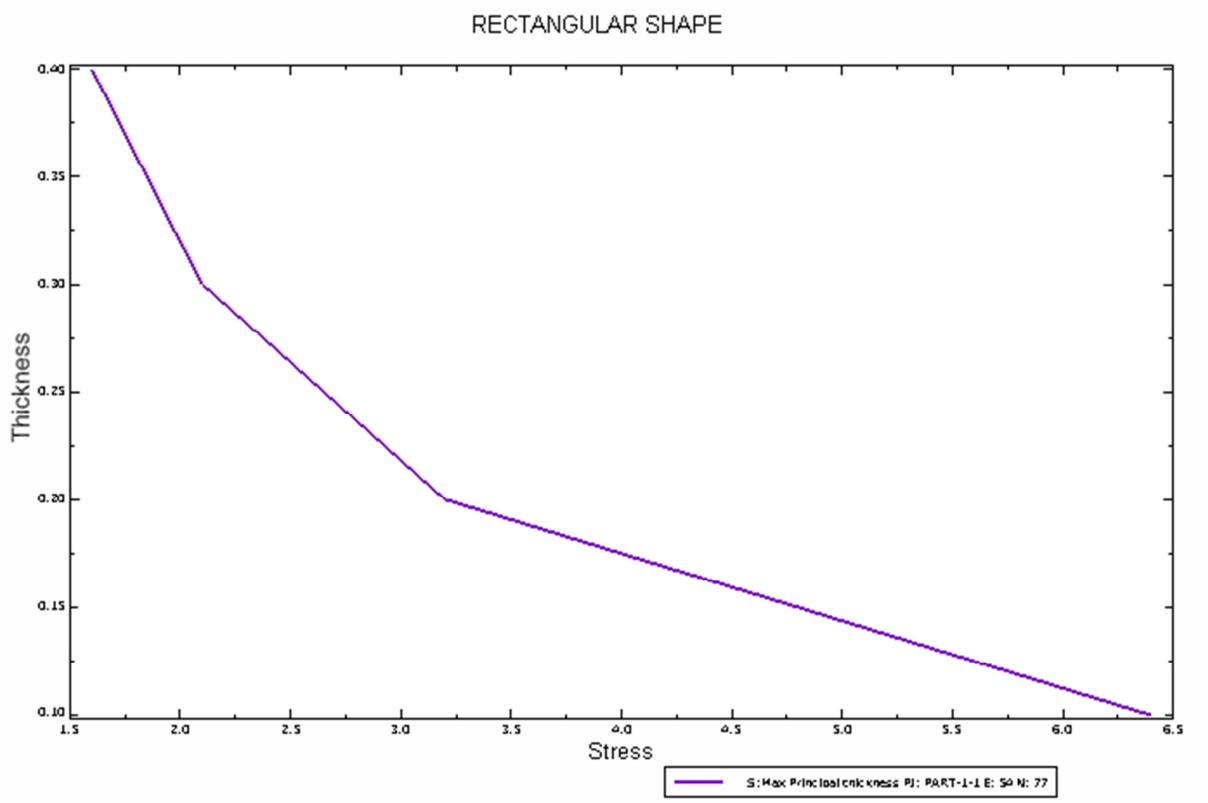
RECTANGULAR SHAPE
Thickness
Stress
S:Max Principal Thickness PI: PART-1-1 E: 50 N: 77

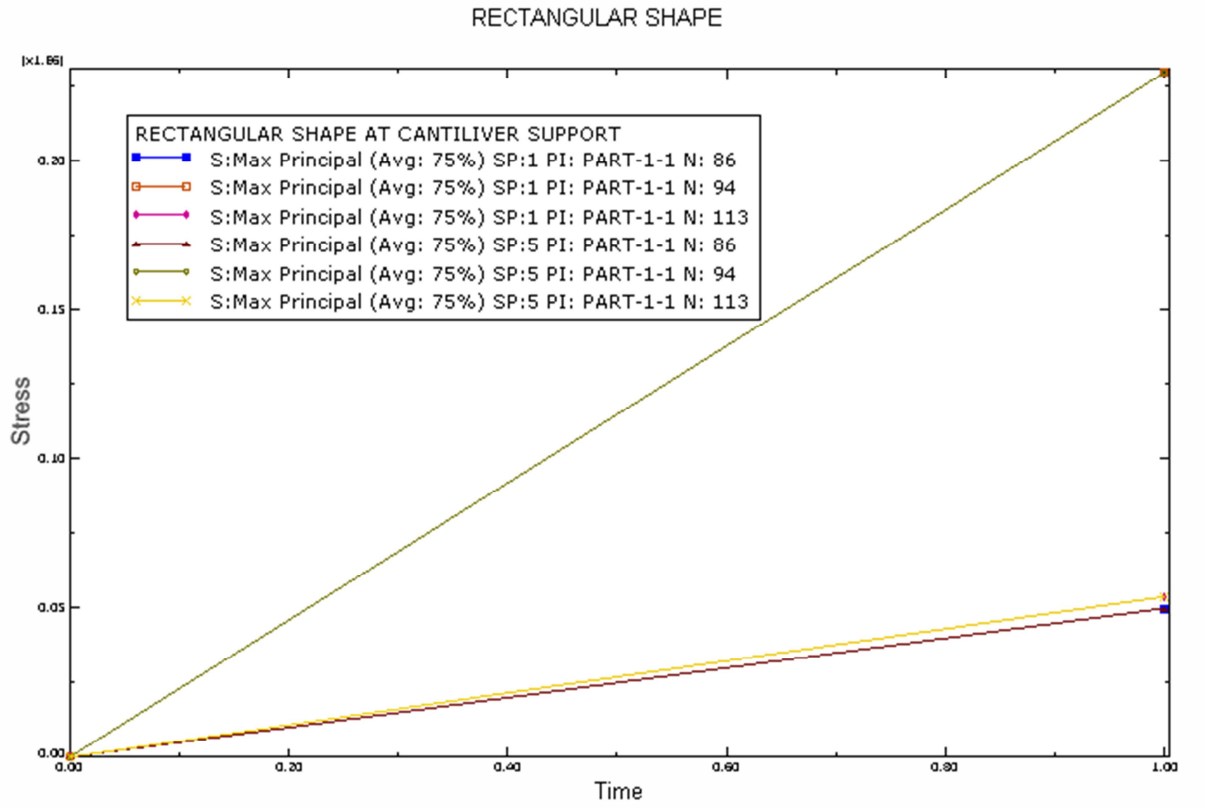
RECTANGULAR SHAPE
[x1.86]
RECTANGULAR SHAPE AT CANTILIVER SUPPORT
S:Max Principal (Avg: 75%) SP:1 PI: PART-1-1 N: 86
S:Max Principal (Avg: 75%) SP:1 PI: PART-1-1 N: 94
S:Max Principal (Avg: 75%) SP:1 PI: PART-1-1 N: 113
S:Max Principal (Avg: 75%) SP:5 PI: PART-1-1 N: 86
S:Max Principal (Avg: 75%) SP:5 PI: PART-1-1 N: 94
S:Max Principal (Avg: 75%) SP:5 PI: PART-1-1 N: 113
Stress
Time

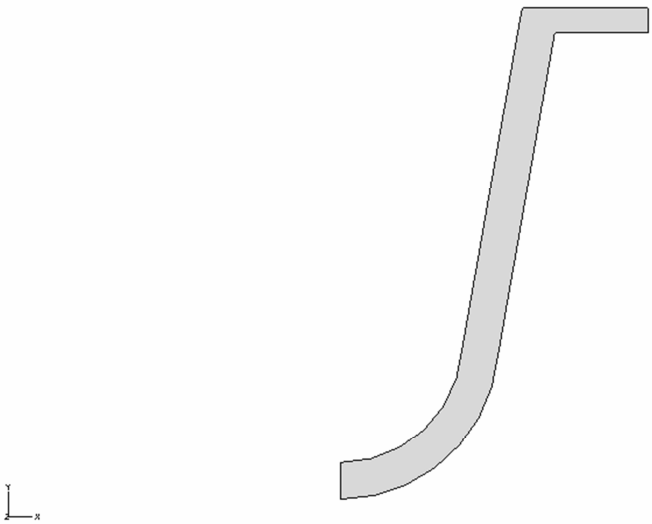

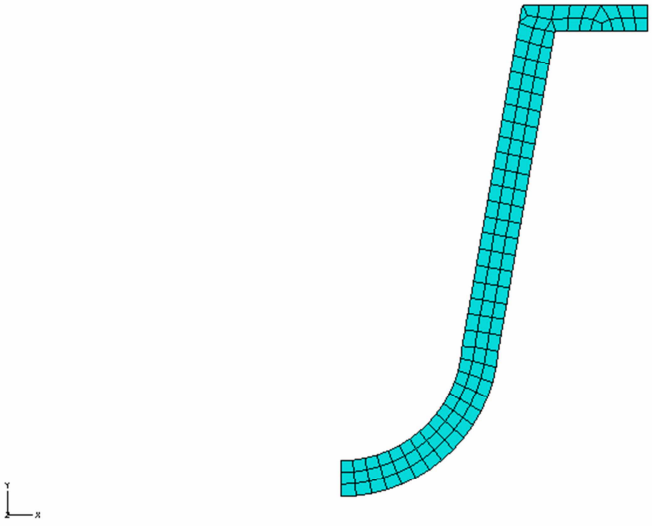

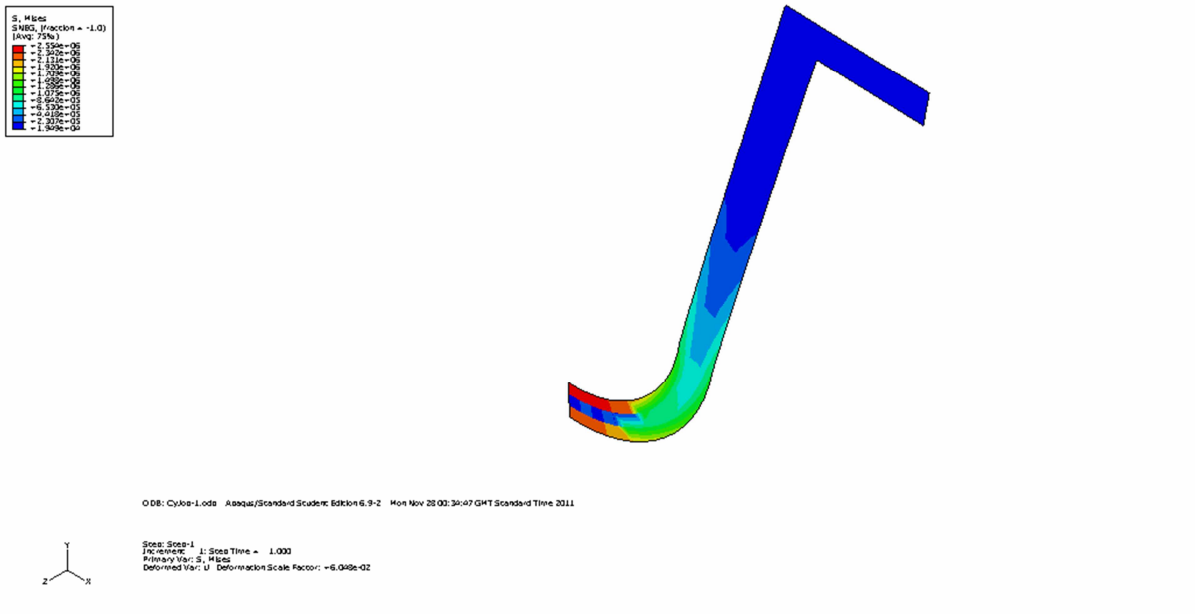

	Min	59.0826E+03	59.0826E+03	-169.677E+03	-169.677E+03	0.	0.
Element		113	113	39	39	113	113
Int Pt		1	1	1	1	1	1
	Maxi	10.2373E+06	10.2373E+06	10.3221E+06	10.3221E+06	10.3221E+06	10.3221E+06
Element		76	76	38	38	38	38
Int Pt		1	1	1	1	1	1
Total		305.098E+06	305.098E+06	170.711E+06	170.711E+06	171.098E+06	171.098E+06

m	35.8568E+03	35.8568E+03	-109.484E+03	-109.484E+03	0.	0.
Element	113	113	39	39	113	113
Int Pt	1	1	1	1	1	1
m	5.11689E+06	5.11689E+06	5.15352E+06	5.15352E+06	5.15352E+06	5.15352E+06
Element	76	76	38	38	38	38
Int Pt	1	1	1	1	1	1
Total	152.257E+06	152.257E+06	85.1968E+06	85.1968E+06	85.3980E+06	85.3980E+06

Minimum	25.3495E+03	25.3495E+03	-83.0752E+03	-83.0752E+03	0.	0.
At Element	113	113	39	39	113	113
Int Pt	1	1	1	1	1	1
Maximum	3.40783E+06	3.40783E+06	3.43086E+06	3.43086E+06	3.43086E+06	3.43086E+06
At Element	76	76	38	38	38	38
Int Pt	1	1	1	1	1	1
Total	101.321E+06	101.321E+06	56.6965E+06	56.6965E+06	56.8356E+06	56.8356E+06

Min	59.0826E+03	59.0826E+03	-169.677E+03	-169.677E+03	0.	0.
Element	113	113	39	39	113	113
Int Pt	1	1	1	1	1	1
Maxi	10.2373E+06	10.2373E+06	10.3221E+06	10.3221E+06	10.3221E+06	10.3221E+06
Element	76	76	38	38	38	38
Int Pt	1	1	1	1	1	1
Total	305.098E+06	305.098E+06	170.711E+06	170.711E+06	171.098E+06	171.098E+06

Minimum	19.4891E+03	19.4891E+03	-66.7367E+03	-66.7367E+03	0.	0.
At Element	113	113	39	39	113	113
Int Pt	1	1	1	1	1	1
Maximum	2.55351E+06	2.55351E+06	2.57041E+06	2.57041E+06	2.57041E+06	2.57041E+06
At Element	76	76	38	38	38	38
Int Pt	1	1	1	1	1	1
Total	75.8860E+06	75.8860E+06	42.4646E+06	42.4646E+06	42.5720E+06	42.5720E+06

CYLINDERICAL SHAPE

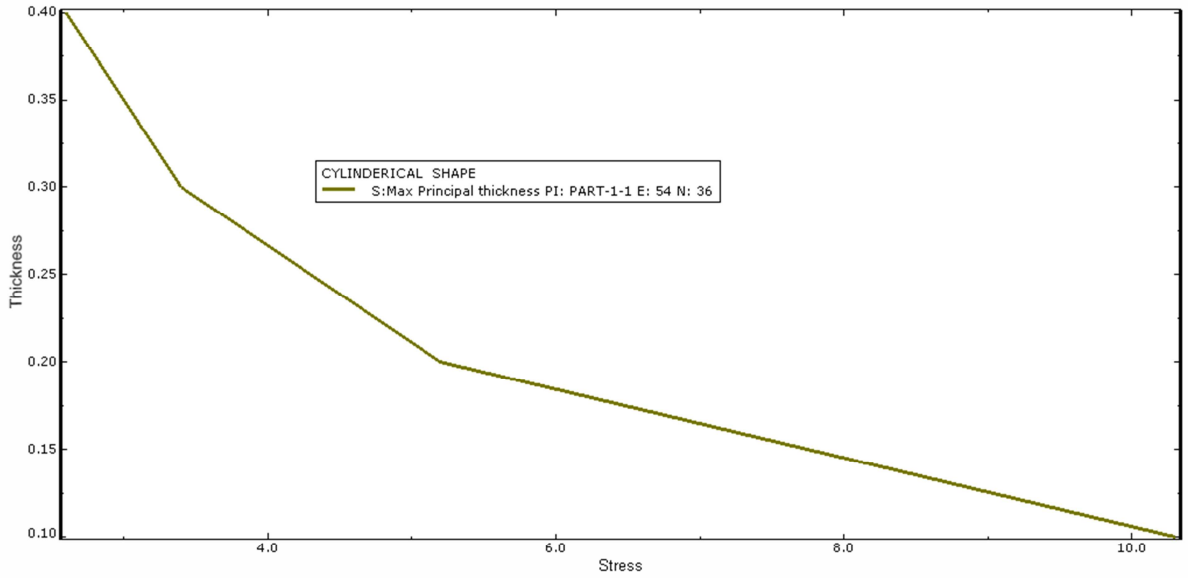

CYLINDERICAL SHAPE

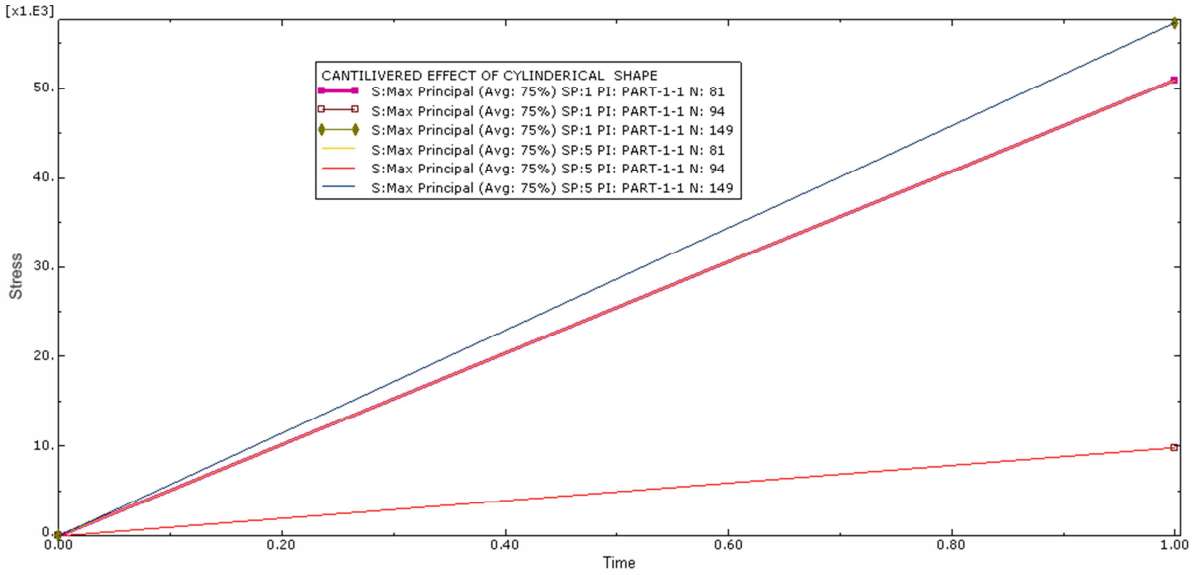

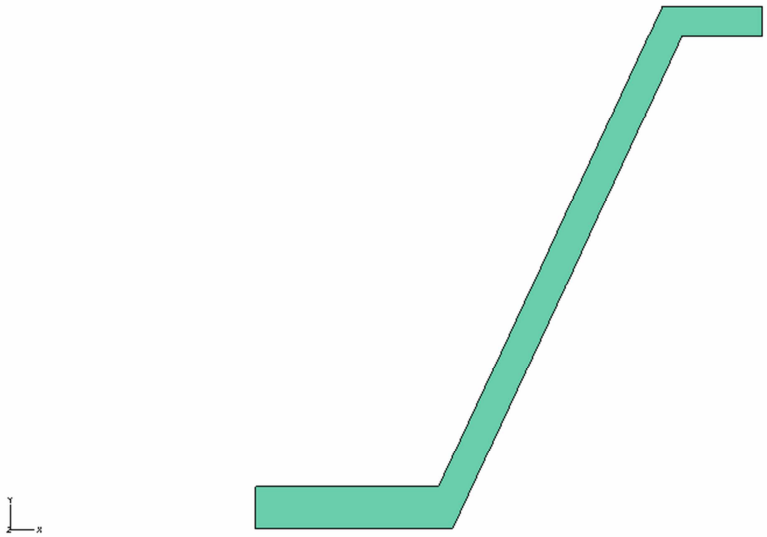

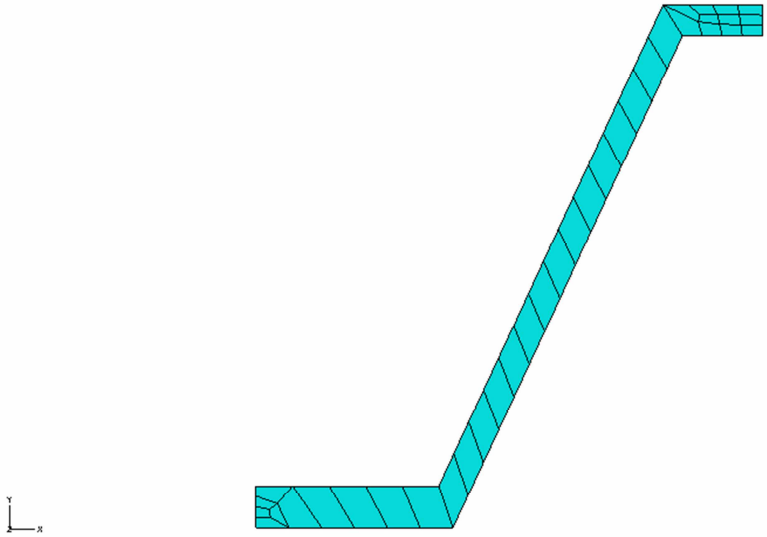

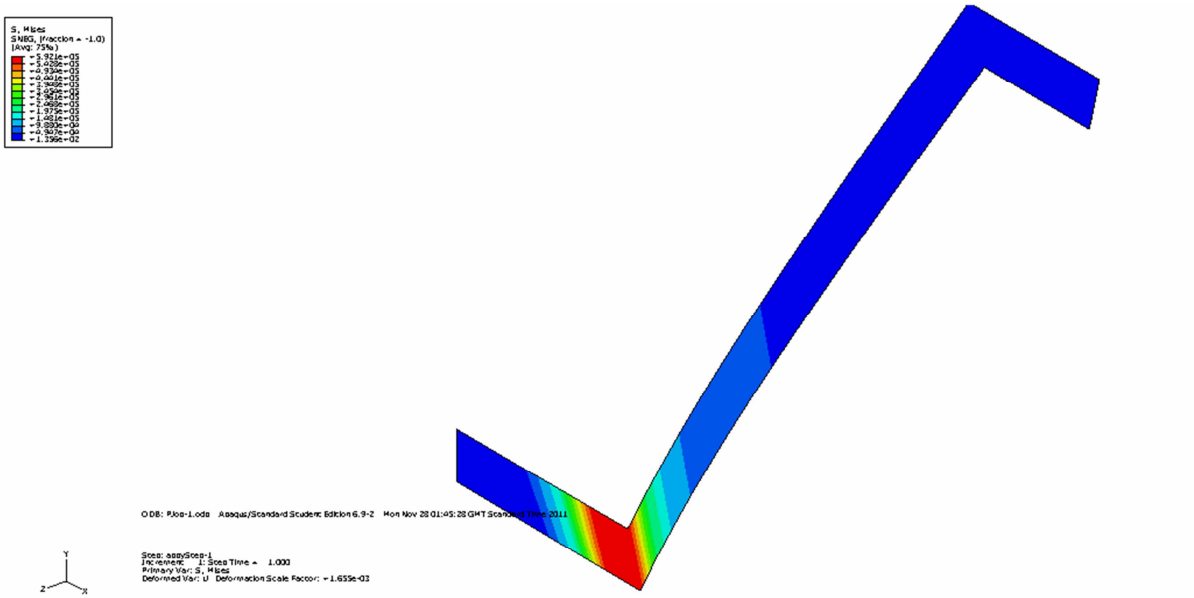

Minimum	10.0068E+03	10.0068E+03	-10.6973E+03	-10.6973E+03	0.	0.
At Element	9	9	31	31	31	31
Int Pt	1	1	1	1	1	1
Maximum	3.327E+06	3.327E+06	2.32773E+06	2.32773E+06	2.32773E+06	2.32773E+06
At Element	13	13	13	13	13	13
Int Pt	1	1	1	1	1	1
Total	11.5793E+06	11.5793E+06	7.79235E+06	7.79235E+06	7.80305E+06	7.80305E+06

Minimum	1.66554E+03	1.66554E+03	-1.85587E+03	-1.85587E+03	0.	0.
At Element	27	27	31	31	32	32
Int Pt	1	1	1	1	1	1
Maximum	1.59358E+06	1.59358E+06	826.195E+03	826.195E+03	826.195E+03	826.195E+03
At Element	13	13	13	13	13	13
Int Pt	1	1	1	1	1	1
Total	4.82520E+06	4.82520E+06	3.11887E+06	3.11887E+06	3.12238E+06	3.12238E+06

Minimum	380.106	380.106	-1.52739E+03	-1.52739E+03	0.	0.
At Element	27	27	8	8	32	32
Int Pt	1	1	1	1	1	1
Maximum	1.0962E+06	1.0962E+06	462.964E+03	462.964E+03	462.964E+03	462.964E+03
At Element	13	13	13	13	13	13
Int Pt	1	1	1	1	1	1
Total	3.10369E+06	3.10369E+06	1.94315E+06	1.94315E+06	1.94527E+06	1.94527E+06

Minimum	135.567	135.567	-1.26274E+03	-1.26274E+03	0.	0.
At Element	27	27	8	8	32	32
Int Pt	1	1	1	1	1	1
Maximum	845.348E+03	845.348E+03	336.317E+03	336.317E+03	336.317E+03	336.317E+03
At Element	13	13	12	12	12	12
Int Pt	1	1	1	1	1	1
Total	2.33540E+06	2.33540E+06	1.42915E+06	1.42915E+06	1.43066E+06	1.43066E+06

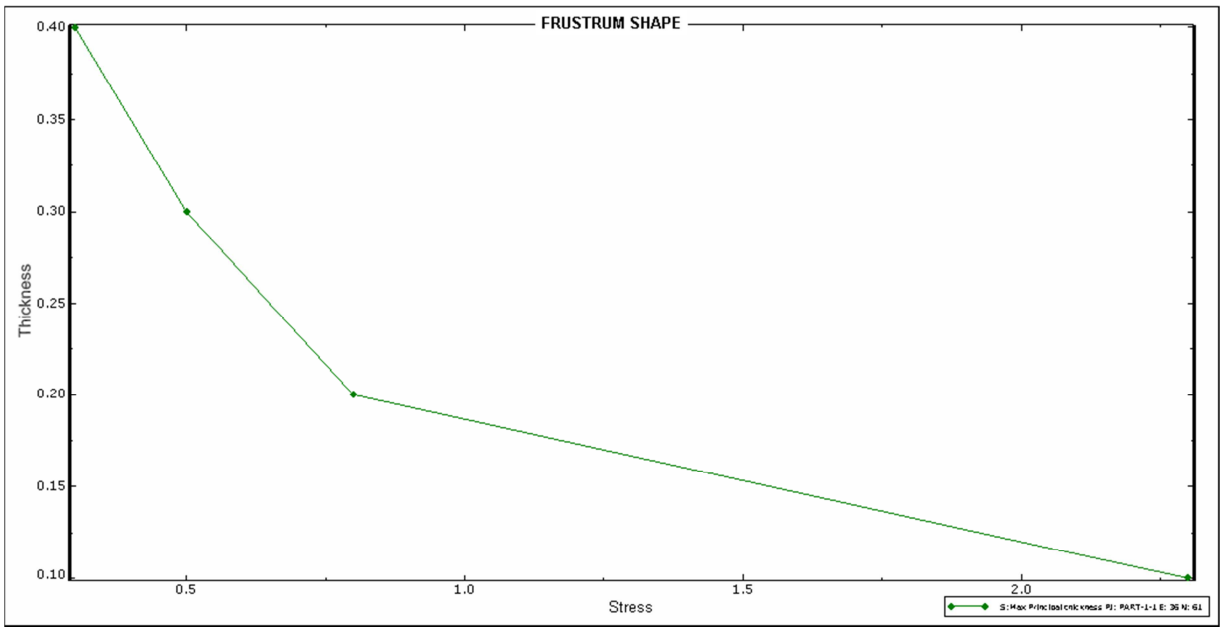

CRACK MODELING

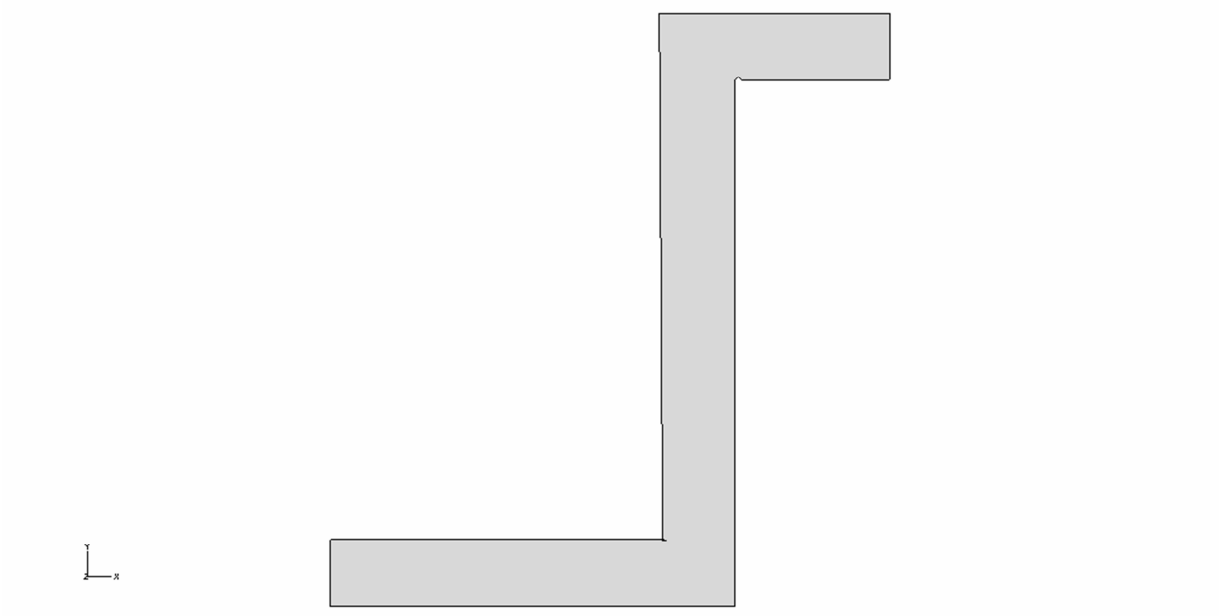

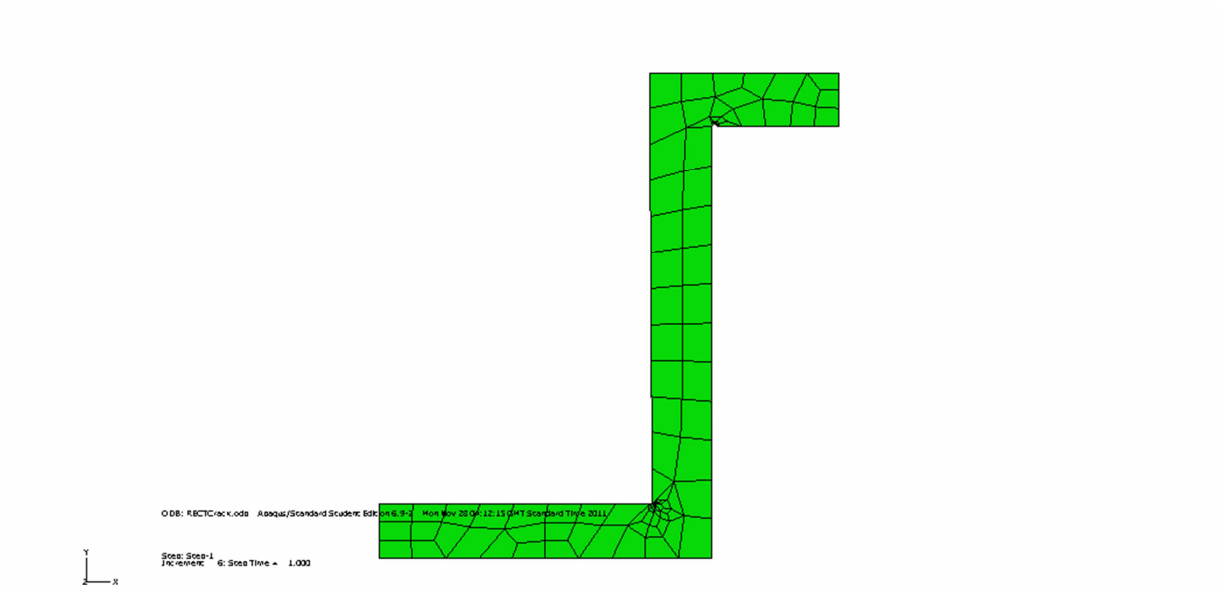

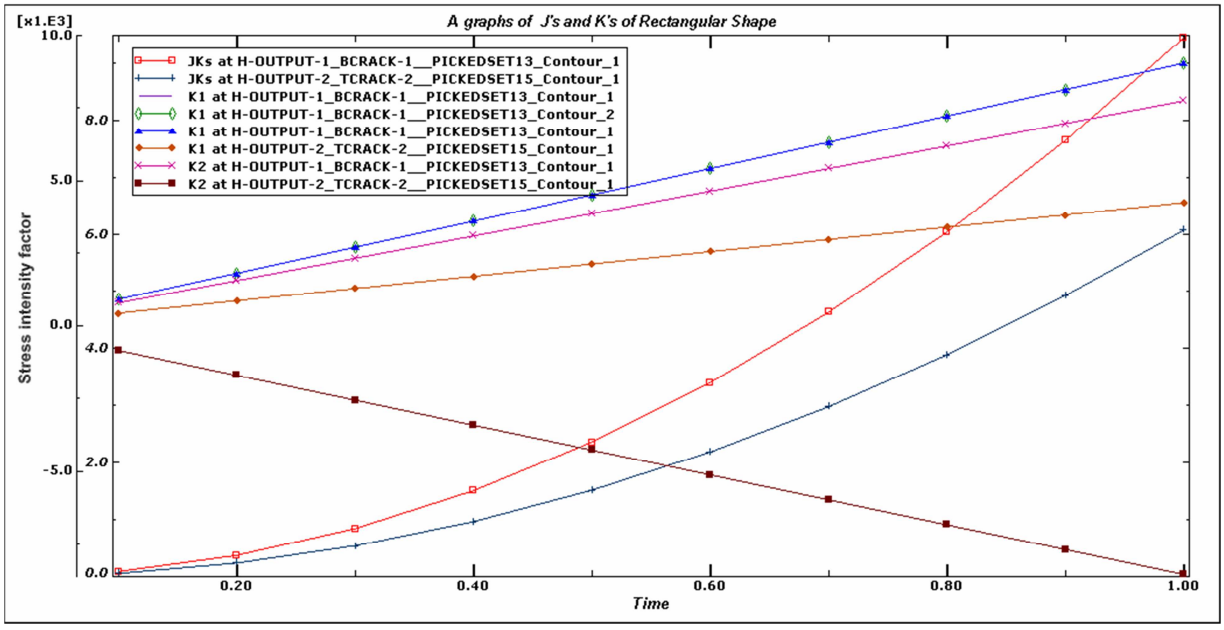
[x1.E3]
A graphs of J's and K's of Rectangular Shape
JKs at H-OUTPUT-1_BCRACK-1__PICKEDSET13_Contour_1
JKs at H-OUTPUT-2_TCRACK-2__PICKEDSET15_Contour_1
K1 at H-OUTPUT-1_BCRACK-1__PICKEDSET13_Contour_1
K1 at H-OUTPUT-1_BCRACK-1__PICKEDSET13_Contour_2
K1 at H-OUTPUT-1_BCRACK-1__PICKEDSET13_Contour_1
K1 at H-OUTPUT-2_TCRACK-2__PICKEDSET15_Contour_1
K2 at H-OUTPUT-1_BCRACK-1__PICKEDSET13_Contour_1
K2 at H-OUTPUT-2_TCRACK-2__PICKEDSET15_Contour_1
Stress intensity factor
10.0
8.0
5.0
6.0
0.0
4.0
-5.0
2.0
0.0
0.20
0.40
0.60
0.80
1.00
Time

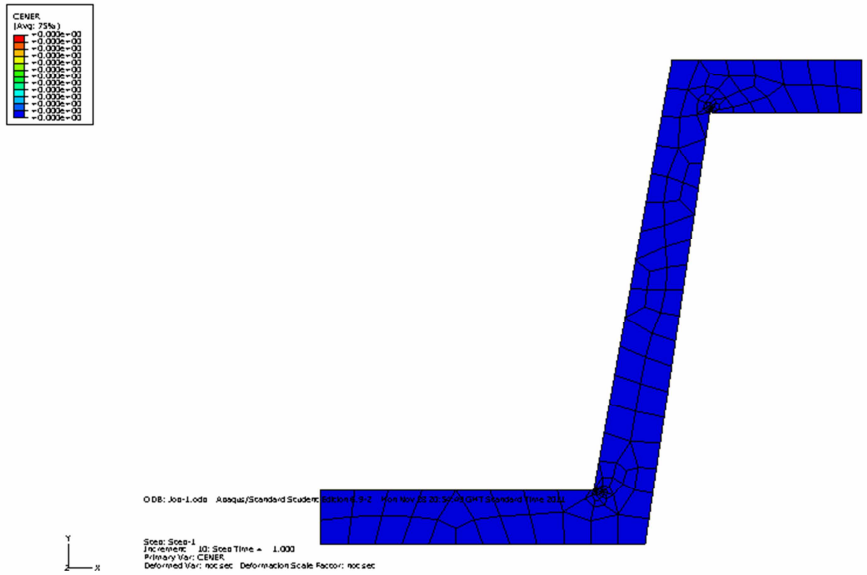
CENER
(Avg: 75%)
ODB: Joa-1.odb Abaqus/Standard Student
Step: Step-1
Increment 10: Step Time = 1.000
Primary Var: CENER
Deformed Var: noc sec Deformation Scale Factor: noc sec

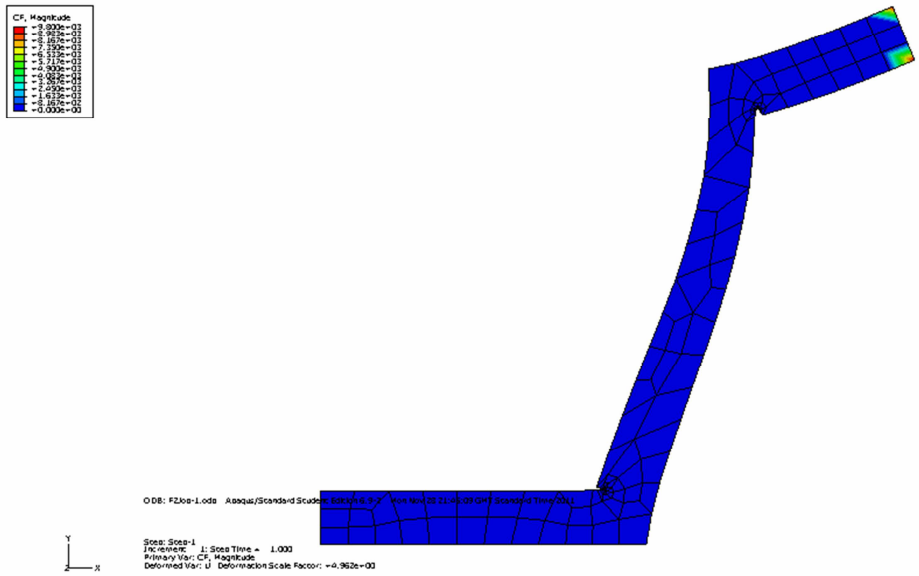
CF, Magnitude
ODB: FZJoa-1.odb Abaqus/Standard Student
Step: Step-1
Increment 1: Step Time = 1.000
Primary Var: CF, Magnitude
Deformed Var: U Deformation Scale Factor: +4.962e+00

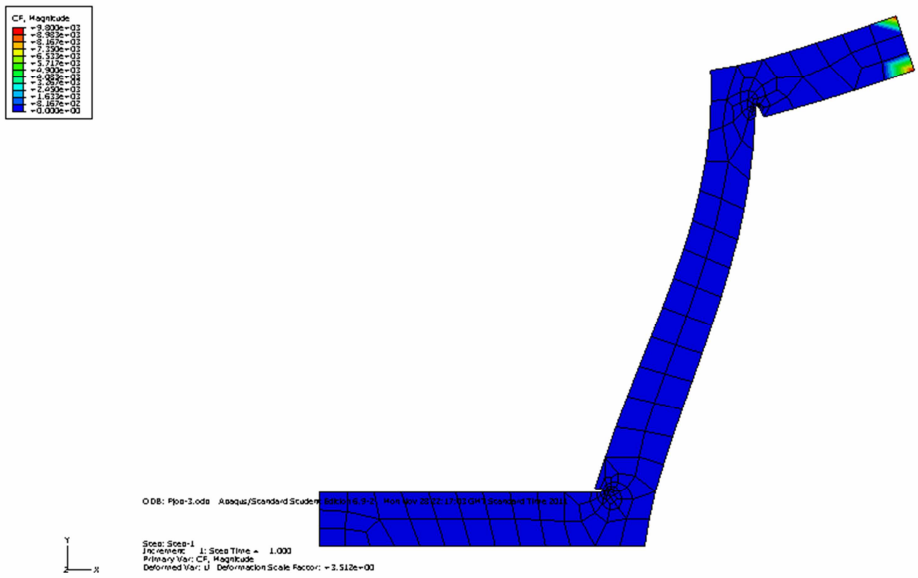
CF, Magnitude
ODB: Fjoa-1.odb Abaqus/Standard Scuden
Step: Step-1
Increment 1: Step Time = 1.000
Primary Var: CF, Magnitude
Deformed Var: U Deformation Scale Factor: +3.512e+00

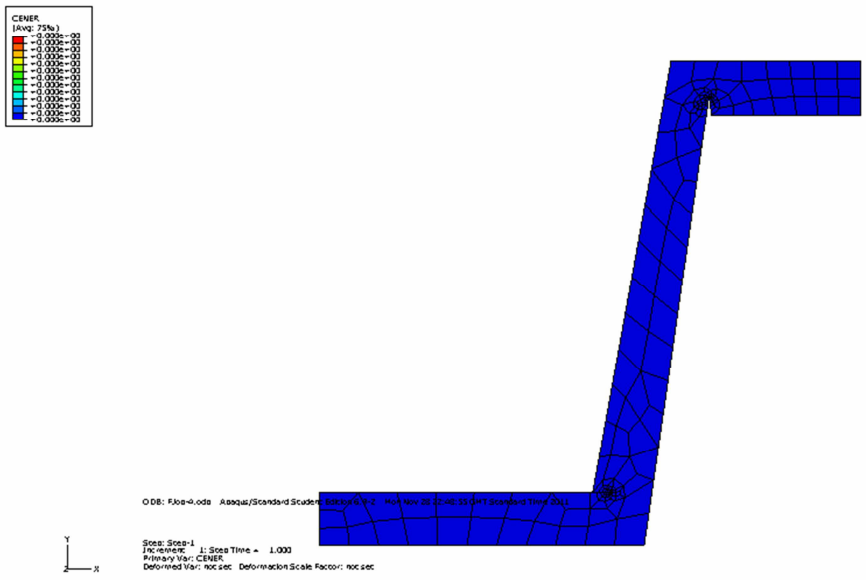
CENER
(Avg: 75%)
ODB: Fjoa-9.odb Abaqus/Standard Scuden
Step: Step-1
Increment 1: Step Time = 1.000
Primary Var: CENER
Deformed Var: noc sec Deformation Scale Factor: noc sec

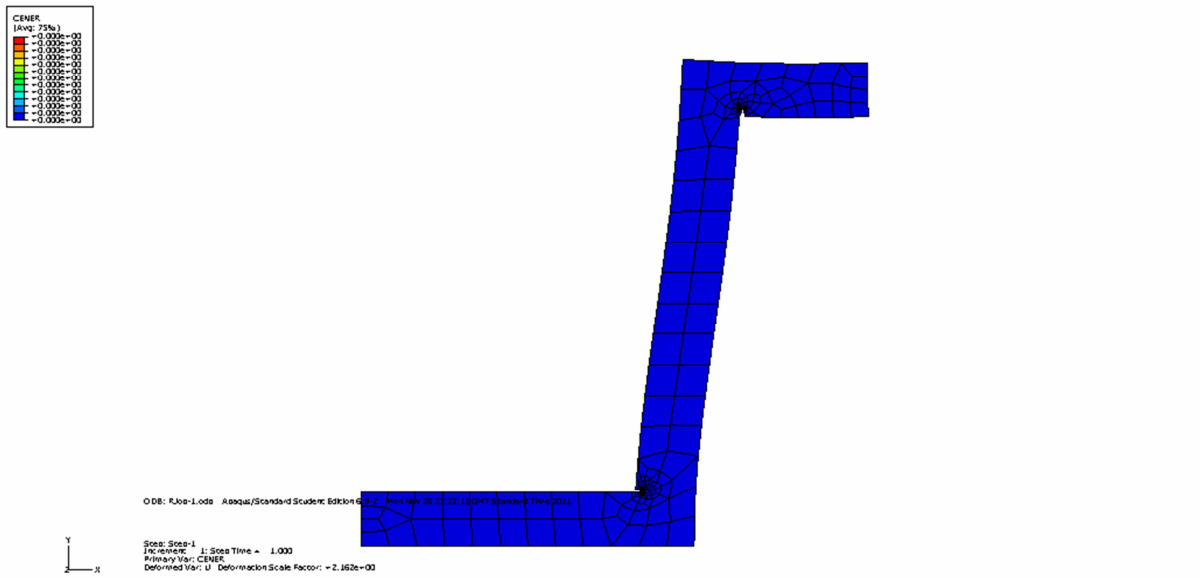
CENER
(Avg: 75%)
ODB: RJoa-1.odb Abaqus/Standard Student Edition
Step: Step-1
Increment 1: Step Time = 1.000
Primary Var: CENER
Deformed Var: U Deformation Scale Factor: +2.162e+00

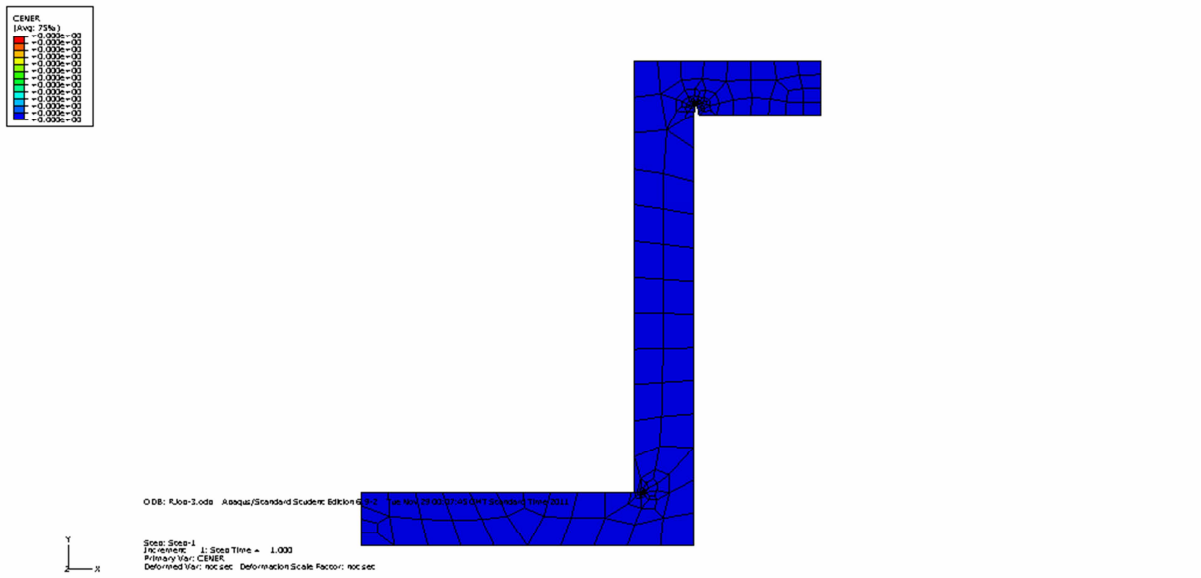
CENER
(Avg: 75%)
ODB: RJoa-2.odb Abaqus/Standard Student Edition
Step: Step-1
Increment 1: Step Time = 1.000
Primary Var: CENER
Deformed Var: noc sec Deformation Scale Factor: noc sec

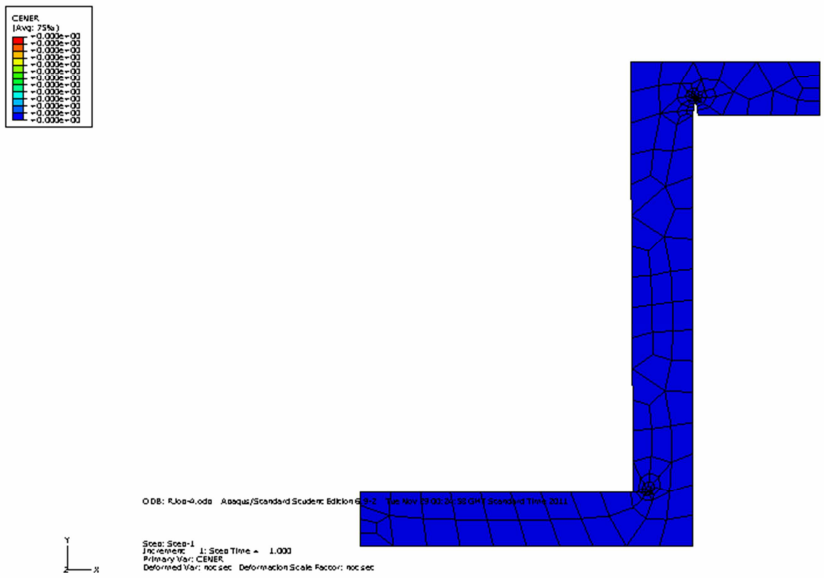
CENER
(Avg: 75%)
+0.000e+00
+0.000e+00
+0.000e+00
+0.000e+00
+0.000e+00
+0.000e+00
+0.000e+00
+0.000e+00
+0.000e+00
+0.000e+00
+0.000e+00
+0.000e+00
ODB: RJoa-0.odb Abaqus/Standard Student Edition 6.9-2
Step: Step-1
Increment 1: Step Time = 1.000
Primary Var: CENER
Deformed Var: noc sec Deformation Scale Factor: noc sec
Y
Z
X

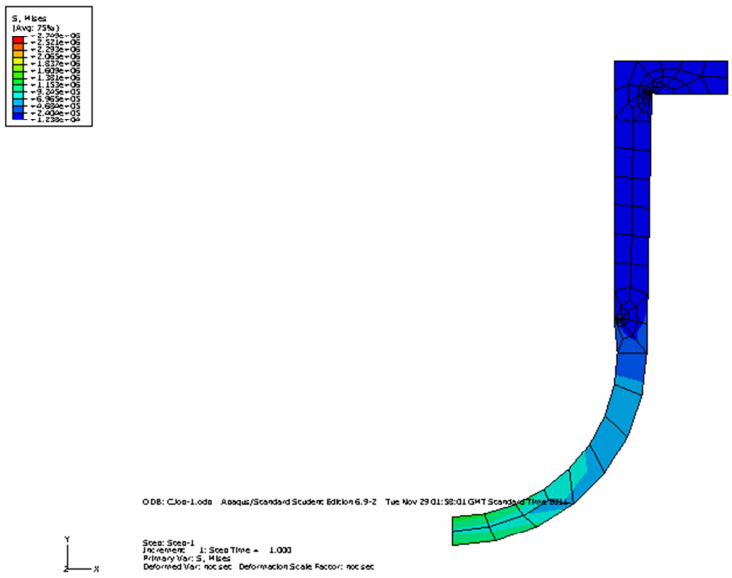
S, Mises
(Avg: 75%)
ODB: CJoa-1.odb Abaqus/Standard Student Edition 6.9-2
Step: Step-1
Increment 1: Step Time = 1.000
Primary Var: S, Mises
Deformed Var: noc sec Deformation Scale Factor: noc sec
Y
Z
X

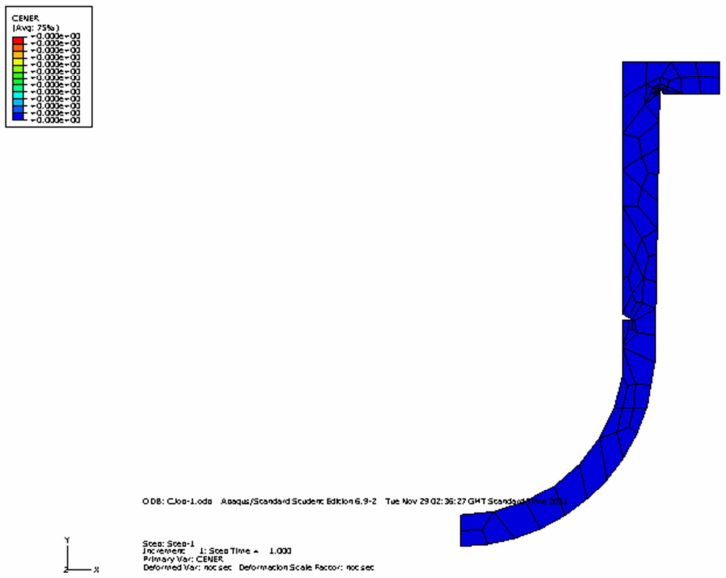
CENER
(Avg: 75%)
+0.000e+00
+0.000e+00
+0.000e+00
+0.000e+00
+0.000e+00
+0.000e+00
+0.000e+00
+0.000e+00
+0.000e+00
+0.000e+00
+0.000e+00
ODB: CJoa-1.odb Abaqus/Standard Student Edition 6.9-2 Tue Nov 29 02:36:27 GMT Standard Time 2011
Y
Z
X
Step: Step-1
Increment 1: Step Time = 1.000
Primary Var: CENER
Deformed Var: noc sec Deformation Scale Factor: noc sec

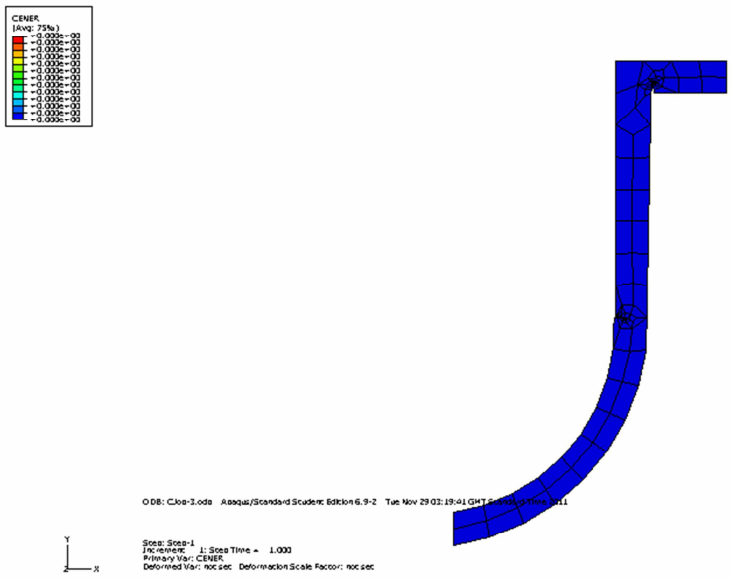
CENER
(Avg: 75%)
+0.000e+00
+0.000e+00
+0.000e+00
+0.000e+00
+0.000e+00
+0.000e+00
+0.000e+00
+0.000e+00
+0.000e+00
+0.000e+00
+0.000e+00
ODB: CJoa-1.odb Abaqus/Standard Student Edition 6.9-2 Tue Nov 29 03:19:41 GMT Standard Time 2011
Y
Z
X
Step: Step-1
Increment 1: Step Time = 1.000
Primary Var: CENER
Deformed Var: noc sec Deformation Scale Factor: noc sec

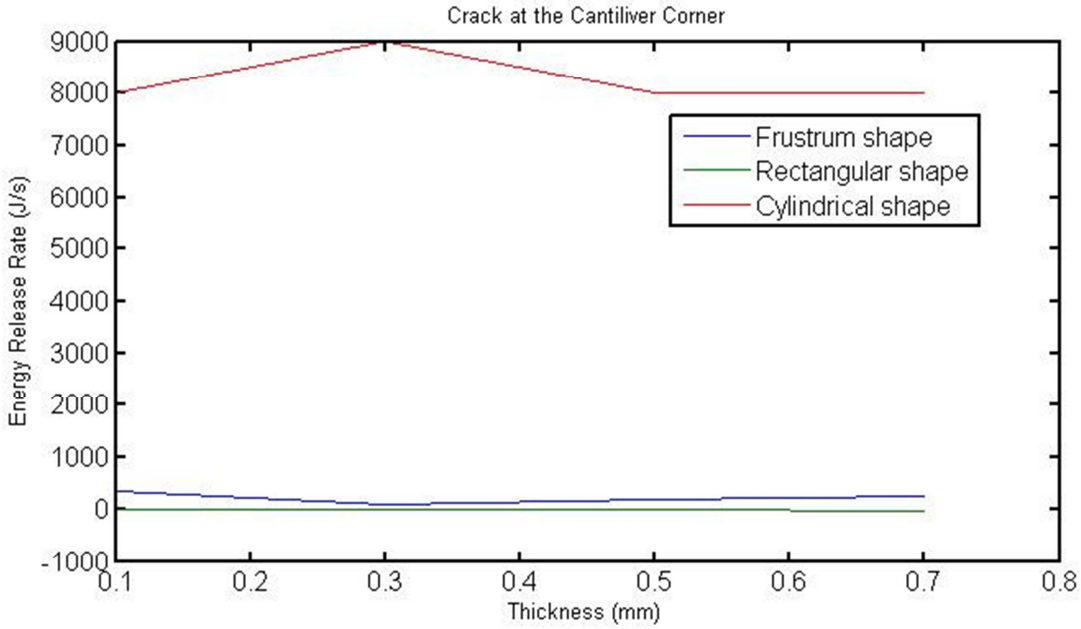
Crack at the Cantiliver Corner
Energy Release Rate (J/s)
Thickness (mm)
Frustrum shape
Rectangular shape
Cylindrical shape
9000
8000
7000
6000
5000
4000
3000
2000
1000
0
-1000
0.1
0.2
0.3
0.4
0.5
0.6
0.7
0.8